

Quantification of Myocardial Macromolecular Transport

By

Jeff M. Hsing

B.S.E., Bioengineering
University of Washington, 1995

SUBMITTED TO THE DEPARTMENT OF ELECTRICAL ENGINEERING AND
COMPUTER SCIENCE IN PARTIAL FULFILLMENT OF THE REQUIREMENTS
FOR THE DEGREE OF

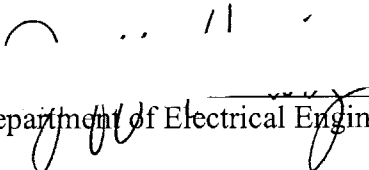
MASTER OF SCIENCE IN ELECTRICAL ENGINEERING AND COMPUTER SCIENCE AT
THE MASSACHUSETTS INSTITUTE OF TECHNOLOGY

JUNE 2000

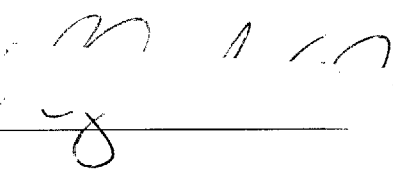
© 2000 Jeff M. Hsing. All rights reserved

The author hereby grants to MIT permission to reproduce and to distribute publicly paper and
electronic copies of this thesis document in whole or in part.

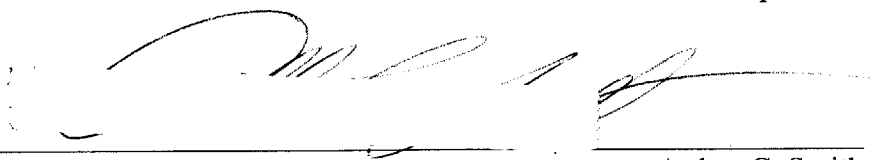
Signature of Author: _____

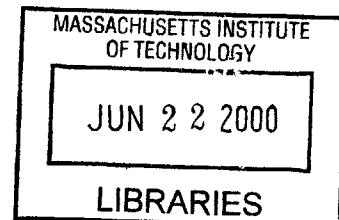

Department of Electrical Engineering and Computer Science
May 19, 2000

Certified by: _____


Elazer R. Edelman
Thomas D. and Virginia W. Cabot Associate Professor
Division of Health Sciences and Technology
Thesis Supervisor

Accepted by: _____


Arthur C. Smith
Professor of Electrical Engineering and Computer Science
Chair, Committee on Graduate Students
of Electrical Engineering and Computer Science



ENG

Quantification of Myocardial Macromolecular Transport

By
Jeff M. Hsing

Submitted to the Department of Electrical Engineering and Computer Science on May 19, 2000
in Partial Fulfillment of the Requirements for the Degree of Master of Science in Electrical
Engineering and Computer Science

ABSTRACT

The needs and impacts of drug administration have evolved from a systemic to a local focus. Local drug delivery would allow a higher local drug concentration at lower systemic toxicity than what can be achieved if delivered systemically. One of the tissues of interest for local delivery is the heart, or myocardium. Increasingly, clinicians are looking to direct myocardial delivery for therapy of complex cardiovascular diseases. Yet, there is little quantitative data on the rates of macromolecular transport inside the myocardium. A porcine model was used in this work as it is most closely similar to humans in size, structure and morphology. Using a technique previously developed in this laboratory to quantify the distribution of macromolecules, the delivery of compounds directly into the myocardium was evaluated. To make quantification generic and not specific for a particular drug or compound, fluorescent-labeled 20kDa and 150kDa dextrans were used to simulate small and large diffusing macromolecules. Diffusion in the myocardium in two directions, transmural and cross-sectional, were investigated to look at diffusion of compounds along and against the myocardium fiber orientation. Fluorescent microscopy was used to quantify concentration profiles, and then the data was fit to a simple diffusion model to calculate diffusivities. This validated the technique developed. The diffusivities of 20kDa dextran in the transmural and cross-sectional direction were calculated to be $9.49 \pm 2.71 \text{ um}^2/\text{s}$ and $20.12 \pm 4.10 \text{ um}^2/\text{s}$ respectively. The diffusivities for 150kDa were calculated to be $2.39 \pm 1.86 \text{ um}^2/\text{s}$ and $3.23 \pm 1.76 \text{ um}^2/\text{s}$ respectively. The diffusivities of the two macromolecules were statistically different ($p < 0.02$ for transmural direction and $p < 0.01$ for cross-section direction). While the diffusion for the larger macromolecule was isotropic, it was not the case for the smaller one. The calculated diffusivity values in the myocardium correlated with previously published data for dextran in the arterial media, suggesting that the transport properties of the myocardium and arterial media may be similar. Applications of quantitative macromolecular transport may include developing novel therapies for cardiovascular diseases in the future.

Thesis Supervisor: Elazer R. Edelman

Title: Thomas D. and Virginia W. Cabot Associate Professor, Division of Health Sciences and Technology

ACKNOWLEDGEMENTS

First and foremost, I would like to thank my thesis supervisor Professor Elazer R. Edelman for allowing to me to join his laboratory and for his supervision of my work. He has been a great thesis advisor as well as a mentor. Despite his extremely busy schedule, he always made time to discuss research and career choices with me. He has provided me with a lot of advice ranging from choosing an interesting thesis topic to advising me on academics as well as personal career choices. His insights were always helpful and encouraged me to think critically about myself and my life's direction.

These past one and a half years would not have been as fun and stimulating if it were not for the people in the Edelman laboratory. I would like to thank everyone for their patience, their teachings, and their ability to entertain me. It was a true learning experience considering the diversity of backgrounds of people in this laboratory. It was the interactions with all the people in the laboratory that made it fun and for me to forget about the sometimes tedious bench work. I would like to thank Chao-Wei Hwang for his help in teaching me all that he knew about fluorescent microscopy. He was always available to help me out with my technical difficulties as well as to answer my questions. I thank David Wu for his constant encouragement and his ability to always to keep me on my toes. He always challenged my hypothesis and theories and made me think through everything very thoroughly. I thank Dr. David Ettenson for always being there and allowing me to ask him random questions ranging from biology to Canada, although he never really answered many of them. A lot of the work would not have been possible if it were not for the guidance and expertise of Phil Seifert in teaching me all that I know about histology and sectioning of tissue. Special thanks to Fardad Hashemi for helping me with Microsoft Word and the formatting of my thesis.

I would like to thank the department of Electrical Engineering and Computer Science and the Rosenblith Graduate Fellowship during my first year here. The financial support allowed me to concentrate on classwork and gave me the time to explore various research laboratories.

I would also like to thank the University of Washington School of Medicine for allowing me to take a leave of absence during my medical curriculum to come here and pursue a graduate degree. I would also like to thank the Magnuson Scholarship that encouraged students to pursue research during their medical training and to provide some financial support that allowed me to come here.

Finally, I would like to thank my parents, Hsu and Tusi Hsing, and sister Karin for all of their love in support in all of my career choices.

TABLE OF CONTENTS

ACKNOWLEDGEMENTS	3
TABLE OF CONTENTS	4
LIST OF FIGURES	6
LIST OF TABLES	7
CHAPTER 1 INTRODUCTION.....	8
1.1 Statement of the Problem.....	8
1.2 Thesis Organization	8
CHAPTER 2 BACKGROUND	10
2.1 Motivation for Research	10
2.2 Previous Work	12
2.3 Embryology of the Heart and Vasculature.....	13
2.4 Anatomy of the Heart and Artery	14
2.5 Measuring Macromolecular Distribution.....	18
2.5.1 Radioactive Technique.....	18
2.5.2 Non-radioactive Technique.....	19
2.6 Benefits of Fluorescence Microscopy.....	20
2.7 Limitations of Fluorescence Microscopy.....	21
CHAPTER 3 FLUOROSCOPY METHOD.....	24
3.1 Tissue Preparation and Diffusion Cell.....	24
3.2 Immobilization and Sectioning.....	26
3.3 Image Acquisition System	27
3.4 Image Processing	28
3.4.1 Basic Post-Image Processing	28
3.4.2 Getting Intensity Profile.....	28
3.4.3 Conversion of Intensity to Concentration	30
CHAPTER 4 DIFFUSION MODEL	32
4.1 Mechanism of Transport.....	32
4.2 Modeling Transport	34
4.3 Simulating PDE Using Crank-Nicolson Method.....	35
CHAPTER 5 QUANTIFICATION OF MYOCARDIAL MACROMOLECULAR TRANSPORT.....	37
5.1 Introduction.....	37
5.2 Materials and Methods.....	38

5.2.1	Tissue Preparation and Diffusion Cell.....	38
5.2.2	Immobilization and Sectioning and Image Acquisition.....	41
5.2.3	Image Analysis.....	41
5.2.3.1	Basic Post-Image Processing.....	41
5.2.3.2	Acquiring Intensity Profile.....	42
5.2.3.3	Conversion of Intensity to Concentration.....	44
5.2.3.4	Calculation of Diffusivity.....	46
5.3	Results.....	47
5.4	Discussion.....	48
CHAPTER 6 CONCLUSION		50
6.1	Accomplishments.....	50
6.2	Future Work.....	51
APPENDIX A: SIMULATING THE DIFFUSION EQUATION USING CRANK-NICOLSON METHOD.....		53
APPENDIX B: EXPERIMENTAL DATA.....		55
APPENDIX C: MATLAB CODE.....		57
REFERENCES.....		66

LIST OF FIGURES

Figure 1: External view of the porcine heart compared to the human heart.....	15
Figure 2: Diagram of the major structures of the heart.....	16
Figure 3: Layers in an artery.....	18
Figure 4: Fluorescence of dextran-FITC degrades upon light exposure.....	22
Figure 5: Florescence of dextran-FITC remains stable if refrigerated	23
Figure 6: Diagram of the myocardium cutting orientation.....	25
Figure 7: Tissue inside a diffusion cell.....	26
Figure 8: Description of getting intensity distribution profile from an image.....	29
Figure 9: H&E stain of porcine myocardium.....	39
Figure 10: High power magnification H&E stain of porcine myocardium.....	40
Figure 11: FITC Fluorescent image (left) and its intensity image.....	42
Figure 12: Intensity distribution profile pre and post shift.....	43
Figure 13: Intensity to Concentration Standard Curve.....	45
Figure 14: Concentration profile of measured versus simulated.....	47

LIST OF TABLES

Table 1: Comparison of the cardiac and arterial structures.....	14
Table 2: Bulk fluid concentration from intensity equation.....	44
Table 3: Free fractional space (ϵ) of dextran-FITC in myocardium.....	46
Table 4: Summary of the calculated diffusivities of dextran-FITC in porcine myocardium.....	47
Table 5: Summary of dextran diffusivities from previous studies compared to values in the myocardium.....	48
Table 6: Experimental Data for Figure 4.....	55
Table 7: Experimental Data for Figure 5.....	55
Table 8: Experimental Data for Figure 13.....	56
Table 9: Experimental data of the diffusivities calculated.....	56

Chapter 1 INTRODUCTION

1.1 Statement of the Problem

Modeling living systems is complicated because numerous factors may affect the system. To begin studying a complicated system, it must be first broken down into smaller simple pieces that are more manageable to deal with. After solving the smaller pieces, one can put all of the pieces back together to give a picture of the entire system. An example of a complicated living system is the transport of macromolecules in tissue. There are many factors or mechanisms affecting the transport of macromolecules ranging from diffusion, to convection, to binding to name a few. Before one can start to break down transport in a living system into simple components, methods of examining and measuring the transport of macromolecules in tissue must be available. Current methods are limited and an improved method needs to be developed to look more specifically and quantitatively at macromolecular transport in tissue. With an improved method, one can more easily start to look at the basic properties of transport in tissue.

1.2 Thesis Organization

This thesis describes the modification of a previous technique developed for vascular tissue to examine macromolecular transport in the myocardial tissue. Chapter 2 describes the motivation for this research as well as work that has been done previously. Chapter 3 discusses the technique of fluorescent microscopy and how it will be used to quantitatively assess the concentration profile. Chapter 4 describes the mathematical diffusion model used to calculate a concentration profile given by varying certain parameters and using the forward-difference method and Crank-Nicolson method to solve for a solution. Chapter 5 describes the main thesis

work and results obtained with discussion and interpretation of the results. Chapter 6 summarizes the work of this thesis as well as future direction and utility of this method

Chapter 2 BACKGROUND

2.1 Motivation for Research

Heart disease has remained the leading cause of morbidity and mortality in the US since 1920 and accounted for the loss of 959,227 lives in the United States in 1996 (AHA 1999). In the US alone, there are approximately 58 million people with some form of cardiovascular disease, approximately 1 in 5 people, and 12 million people with coronary heart disease (NHLBI 1998). Cardiac arrhythmia also affects millions of people in the US with the first line of treatment being drug therapy. Significant research has gone into trying to find better therapeutic options for heart disease and heart arrhythmias. The most common treatment option is still pharmacological. Over the years, pharmacological agents have improved in their potency and ability to target specific aspects causing the disease. On the horizon of new therapy options include gene therapy, cell transplantation and angiogenic growth factors (Tice 1997).

Delivery of pharmacological agents is not straightforward. The pharmacokinetics of a drug results in one of three outcomes: entry into the tissue of interest, metabolism and clearance by the kidneys or liver, or storage in tissue like fat. Systemic delivery, oral or intravenously, is the easiest route of administration. These modes of delivery rely on the drug entering the blood stream, traversing the entire body with the hope that some of the drug will get to the tissue of interest. The problems with the systemic approach are that there is limited control over the amount of drug that reaches the target tissue and compounds often possess narrow therapeutic ranges, short half-lives, and systemic side effects. Consequently, there has been more focus on

local drug delivery designed to provide therapeutic concentration of drugs for prolonged periods of time only to the tissue of interest without systemic side effects (Bailey, 1997).

To optimize local drug delivery, there is a need for a method to quantify and characterize the amount of drug or compound delivered into the tissue by the delivery device. A method has been developed in our laboratory to quantify and characterize the amount of a compound that is delivered to vascular tissue. A natural extension to quantifying transport through vascular tissue is to quantify transport through myocardial tissue. It is not clear whether the properties of myocardium are similar enough to that of the vasculature to allow for inference of transport mechanisms.

In an *in vivo* system, there are many factors that are involved in the transport of macromolecules once the drug enters the tissue of interest. A full detailed description of the various transport mechanisms is included in chapter 4. In an *in vivo* system, all transport mechanisms come into play and complicate the ability to quantify the contributions of each mechanism. To simplify a complicated system, each component will be examined individually, starting with diffusion. By focusing exclusively on diffusion, the other factors will be held constant or removed entirely. *Ex vivo* systems allow one to examine bulk diffusion in isolation without convection, electrodiffusion, or the effects of the beating heart.

Quantitative tools to assess distribution of molecules have been hindered by post-experiment artifact, low signal-to-noise ratios, poor spatial resolution, and inability to provide multi-dimensional drug distribution profiles. A better method to look at transport in the tissue is therefore required. Once a better technique to assess and quantify the distribution of macromolecules in the tissue is available, a better evaluation of the delivery device or method and to evaluate its transport mechanism can be made.

2.2 Previous Work

There has been limited work characterizing transport of macromolecules in myocardial tissue. Some have examined drug entry into vascular tissue and attempted to extrapolate the same analysis to myocardial tissue. Such an approach may not be valid since the macro and ultrastructure of myocardium and vasculature are at times similar and different and they will be discussed below.

Transport studies in the myocardium have focused primarily on oxygen transport and diffusion from the capillaries into the myocardium. Elaborate experimental models and mathematical models have been developed in assessing oxygen transport time from the capillaries into the tissue (Popel 1989, Wolpers et al 1990, Van Beek et al 1992, Nemato 1997). Previous studies of transport of other macromolecules have generally been qualitative rather than quantitative. Current research has been more focused on the design aspects of delivery catheters, endovascular stents, polymeric implants, extravascular polymeric wraps, and injectable microspheres (Kornowski 2000, Avitall 1992, Arras 1998). Studies by Haunso and Host in 1990 and 1996 have shown that transport of beta-blockers, calcium antagonist, and aminoterminal propeptide of Type III procollagen in cat myocardium was significantly slower when compared to free diffusion in water. Fluck et al in 1998 looked at solute exchange in rabbit myocardium of different disease state. But otherwise, little quantitative work has been done in this field.

One of the potential applications for quantifying transport in myocardial tissue is for the local delivery of angiogenic factors to the heart. Many clinical studies have used angiogenic factors like fibroblast growth factor-2 (FGF-2, bFGF) and vascular endothelial growth factor (VEGF) for local drug delivery (Edelman, Nugent et al 1993, Lopez et al 1997). These studies mainly reported the end effects of whether there was any increase in coronary perfusion or

improvement in clinical symptoms. But few have looked quantitatively at the transport, deposition and distribution of growth factors in the myocardium. For all the angiogenic studies, there is an assumed link that the growth factors, delivered by whatever method actually reaches the site of interest. Limited work has been done to demonstrate conclusively that the growth factors are actually present and remain there to cause the angiogenic effects. One reason for the lack of study is that there have been limited tools to rigorously assess macromolecular transport.

2.3 Embryology of the Heart and Vasculature

It has been said that the heart is in fact just a large blood vessel. This statement can be made since the embryological origin of the vasculature and heart are the same. To understand the basic anatomy and ultrastructure of the heart and vasculature and to make comparisons, it is important to look at and compare the embryology of the heart and vessels. Embryologically, the heart and blood vessels come from cells of similar origin, from angiogenic cluster cells, which arose from the mesenchyme. The cardiovascular system is the first system to function in the embryo, with blood circulating by the end of the third week (Moore, 1988). The earliest sign of the heart and vessels can be seen when mesenchymal cells in the splanchnic mesoderm layer form isolated “angiogenic clusters.” These clusters aggregate and arrange themselves side-by-side to form two longitudinal cellular strands called cardiogenic cords. The two cords canalize to form thin-walled endothelial tubes called endocardial heart tubes. Further development leads to the fusing of the two into a single heart tube. As the heart tubes fuse, the mesenchyme that surrounds them thickens to form the myoepicardial mantle. At this point, the developing heart is an endothelial tube, separated from the myoepicardial tube by a gelatinous connective tissue called the cardiac jelly. The endocardial tube becomes the endocardium, and the myoepicardial

mantle becomes the myocardium and the epicardium. Thus the three layers of the heart are formed (Langman, 1981).

A similar process occurs with the blood vessels as the vascular system is derived from the same cluster of cells as the heart. The angiogenic cells that form the primitive heart form the main branches of the aortic arches and the common cardinal vein. The heart tube and vessels are connected at an early stage. As the vessels evolve, mesenchyme cells aggregate and surround the arteries forming the three layers similar to the heart. The initial tube evolves to become the endothelial lining of the arteries, and the mesenchymal cells become the media and adventitia.

From an embryological standpoint, the following anatomy of the two structures is derived from similar cells and thus some comparisons between the two can be made. A summary is shown in Table 1.

Embryonic Structure	Heart Structure	Artery Structure	Embryonic Structure
Endocardial tube	Endocardium	Endothelium	Vessel tube
Myoepicardial mantle	Myocardium	Media	Mesenchyme cells
Myoepicardial mantle	Epicardium	Adventitia	Mesenchyme cells

Table 1: Comparison of the cardiac and arterial structures.

2.4 Anatomy of the Heart and Artery

The porcine model has been widely used in cardiovascular research, as the pig heart resembles the human in size, shape, structure, and morphology (Crick SJ, 1998, Weaver ME 1986). Thus, it is felt that experiments done with the porcine model can be easily extended to the human. Figure 1 shows a side-by-side gross picture of the porcine and the human heart.

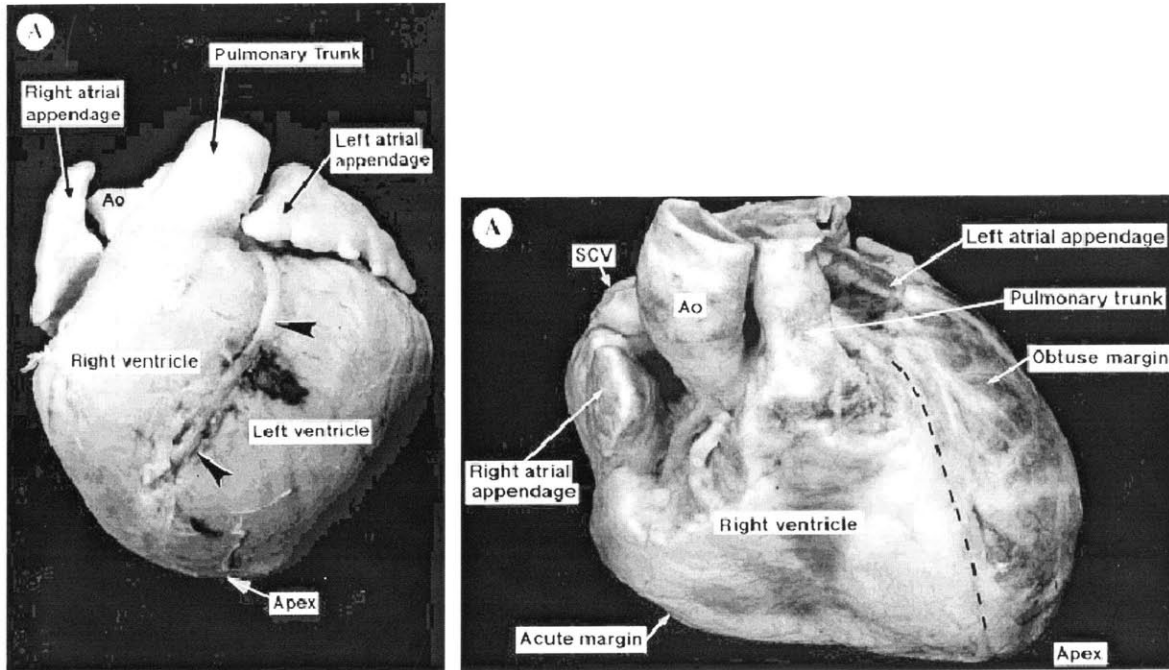


Figure 1: External view of the porcine heart (left) compared to the human heart (right).
 (Crick SJ, Et al)

Both the human and pig hearts are composed of four main chambers, the right and left atrium, and right and left ventricles. Deoxygenated blood from the superior and inferior vena cava flows into the right atrium, through the tricuspid valve into the right ventricle, and then through the pulmonary valve into the pulmonary arteries to the lungs for oxygenation. Oxygenated blood returns from the lungs through the pulmonary veins into the left atrium, through the mitral valve into the left ventricle, and through the aortic valve before being pumped out to the aorta to the rest of the body. Two small orifices, or ostia, course off the base of the aortic valve and outflow tract of the aorta and these give rise to the coronary arteries. Since the left ventricle is the chamber that is most responsible for delivering blood to the entire body, it is usually the thickest, most musculature and most powerful of all the chambers. Many diseases affect the left ventricle and it is usually the target for angiogenic therapy. The muscle wall is divided into three layers, the endocardium, myocardium, and epicardium. The endocardium is

the innermost layer of the heart and it contains a layer of squamous epithelium that forms the barrier between the ventricle and myocardium with subendothelial connective tissue. The myocardium is composed mainly of cardiac muscle cells arranged into fibrous sheets separated by facial planes and it is these cells and their arrangement that provides the strength of heart contraction. They are tightly packed to form muscle sheets and groups of cells are arranged in bundles surrounded by fascial sheaths. Both the muscle sheets and fascial sheaths serve as potential transport barriers in the transmural direction. The epicardium is the outermost layer containing the fatty connective tissue outside the heart and the large coronary vessels. Figure 2 shows the major structures of the heart.

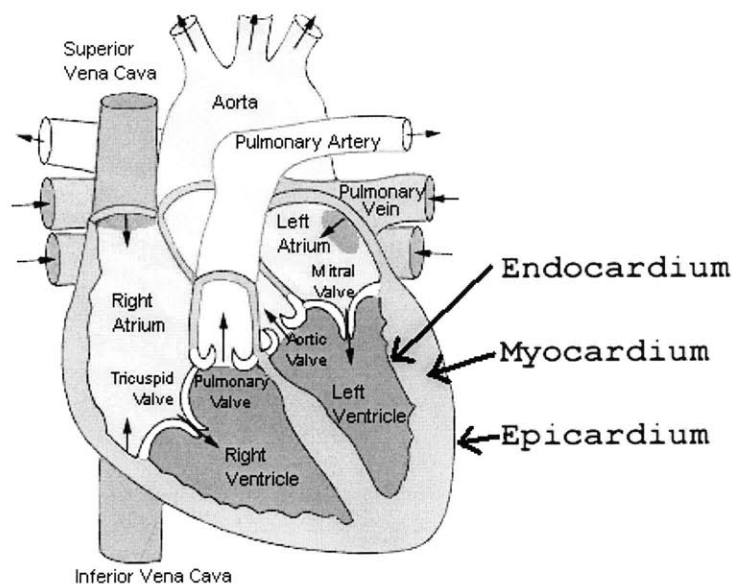


Figure 2: Diagram of the major structures of the heart. The major structures of the heart are labeled including the endocardium, myocardium, and epicardium which as the 3 layers of the muscle wall.

The heart muscle is composed of cardiac muscle cells, which differ from both the body's volitional skeletal muscles and involuntary smooth muscle. Arterial smooth muscle cells are in the latter groups. Cardiac cells are unique in that they are relatively short, thick, mononuclear, and are branched. This configuration optimizes their function as impulse generating, conducting,

and responsive elements. These muscle cells are arranged into three muscle planes, wrapping around from left to right to form the shape of the heart. In general, the muscle layers are oriented more horizontally than vertically. The first layer is a nearly horizontal and forms the innermost muscle layer of the left ventricle. The next two layers are oriented more slightly downward, wrapping the heart to form the right and left ventricles (Katz 1992). The arrangement of the cardiac muscle fibers are oriented such that that when it contracts, the ventricles are squeezed like a clenched and unclenched fist.

The vasculature is divided into arteries that bring blood away from the heart and veins that carry blood back to the heart. The artery is composed of three morphologically distinct concentric layers that are derived from different types of cells embryologically. The innermost layer, the tunica intima, is composed of a monolayer of endothelial cells supported by the internal elastic lamina, connective tissue composed mainly of elastin. In larger species, vascular smooth muscle cells can be arrayed in tunica intima as well. The middle layer, the tunica media, is composed of circumferentially aligned smooth muscle cells with thin sheets of connective tissue collagen and elastin interspersed in between. The smooth muscle cells contract and relax to modulate downstream blood flow depending on conditions and signals. The outermost layer is the tunica adventitia, separated from the media by a fenestrated sheet of elastin and composed mainly of type I collagen with loosely arranged fibroblasts and smooth muscle cells. A diagram of the layers of the artery is shown in Figure 3.

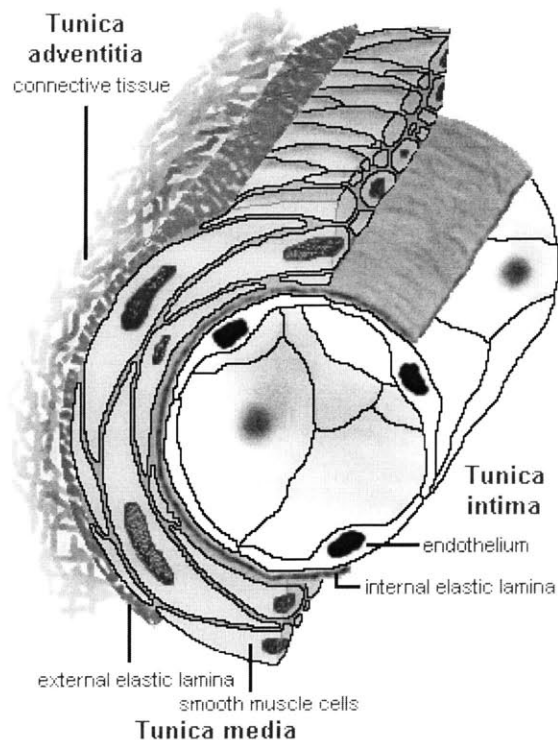


Figure 3: Layers in an artery. There are three layers that form the artery: tunica intima, tunica media, and tunica adventitia.

2.5 Measuring Macromolecular Distribution

Two commonly used techniques have been employed to quantify macromolecular distribution, radioactive and non-radioactive methods. A brief description of both will be presented here along with an explanation for this thesis' use of a non-radioactive technique.

2.5.1 Radioactive Technique

Most pharmacokinetic research in the past tracked the movement and distribution of compounds by radioactive methods. Commonly used radioactive nucleotides that can be attached to the compound of interest to track its movement include tritium (^3H) and iodine (^{125}I). Once the radioactive compound is attached, tracing the movement and concentration profile of the compound can easily be detected by scintillation or radiographically. Radioactivity counts of the compound or intensity on exposed film can be converted to physical concentrations if the

specific activity of the radiolabel is known. Yet, radioactivity has limited spatial resolution and potential health hazards and issues of environmental protection and disposal. Spatial resolution limitation occurs because detection of radiation requires exposing the radioactivity to film over an extended period of time. Then the film is used to visualize the distribution of radioactive materials. Since radiation is emitted in all directions, the image on the film is a composite signal from sources nearby thus limiting the resolution. With radioactivity, there is a trade off between signal-to-noise ratio and resolution. The higher your signal-to-noise ratio, the lower the resolution that is obtainable.

However, radioactive technique to measure drug distribution is widely used in research laboratories as previous work in our laboratory has examined transmural transport of tritium-labeled heparin through the rat abdominal aorta with success (Lovich and Edelman 1995). Other work in our laboratory has also used iodinated dextran molecules to measure its transport across arterial wall (Elmalak and Edelman 2000).

2.5.2 Non-radioactive Technique

Transport and molecular studies have also utilized non-radioactive markers including Evans-blue, horseradish peroxidase, fluorescent tags fluorescein isothiocyanate (FITC) and rhodamine B. Similar to radioactive tags, the non-radioactive tags attach to the compound of interest. Detection of non-radioactive markers either involves looking at color change of the compound or using fluorescence to detect the presence of the fluorescent markers. Fluorescence results from emission of energy by a molecule when excited by an external energy source. Molecules, which have this capability, are usually called fluorophores. Two in particular that are widely used are FITC and rhodamine B. Fluorophores usually absorb energy at a particular wavelength, which excites electrons into a higher energy state. Then shortly after (1-10 ns), the

electron in the excited state emits a photon of energy and returns to the ground state. Thus, to detect fluorescence, a particular wavelength of light that corresponds to the energy that the molecule absorbs is illuminated onto the molecule. A detector detects the wavelength of light that the molecule emits when the electron energy state returns from an excited state to ground state.

The most commonly used fluorescent tag in transport studies is fluorescein isothiocyanate (FITC). FITC is a small (389 dalton) neutral and polycyclic molecule that is maximally excited at 492nm wavelength and emits energy above 530nm wavelength. Its small size makes it less likely to affect the transport of the compound to which it is attached. As FITC rarely interfere with transport and binding, it is commonly used in tissue transport studies.

2.6 Benefits of Fluorescence Microscopy

There are advantages in choosing fluorescence technique over a radioactive one. One of the major benefits of using non-radioactive labels is the avoidance of health and environmental hazards. Use of radioactivity requires all users to go through radiation safety training as well as special facilities to accommodate and dispose of radioactive materials and waste. There is also radiation exposure hazard to the researchers that is not present in using fluorescent-labeled markers. Spatial resolution of fluorescence markers is much better than radiation. Detecting fluorescence requires exciting the molecule with a certain wavelength of light and detection is based on a fluorescent microscope and digital camera. Since fluorescent images are captured instantaneously, there is minimal resolution degradation due to long film exposure as is encountered in autoradiographic methods. In addition, the ability to tag different color fluorescent markers to molecules is another advantage. Different color fluorescent markers can be resolved using specific passband filters. This allows the ability to simultaneously image two

separate macromolecules. This is difficult to accomplish using radioactive methods. Our laboratory previously has shown that fluorescent markers (FITC) attached to dextrans can be used as a superior method to quantify the distribution of macromolecules in the vascular tissue (Wan, Lovich et al, 1999).

2.7 Limitations of Fluorescence Microscopy

As with all techniques, there are limitations as well. One of the major drawbacks of non-radioactive technique is the lack of a uniform standard curve that can be used to calculate concentrations from intensities. Whereas radioactive counts are a good indicator of concentration, the same cannot be said for fluorescence. The intensity of the source excitation light plays a role in determining the intensity of fluorescence. Consequently, a standard concentration curve must be created each time fluorescent images are acquired. Image size is another limitation to fluorescence. Fluorescence requires the area of interest to be excited by light of a particular wavelength. Usually fluorescence microscopy is performed where the light source only needs to excite a small area, and problems arise when a large area needs to be excited at a particular wavelength of light. For large whole tissue samples, like the myocardium, generating a large uniform light source is difficult. Specially designed large-scale fluorescent imagers are needed to look at large tissues. In radioactivity, the size is limited by the size of the film, and large film sizes are readily available.

Photobleaching is another limitation of fluorescence. Over time, as the fluorescent marker is exposed to light, the marker loses its ability to fluoresce. This can be seen in Figure 4 where dextran attached to FITC was exposed to room light and its fluorescence was examined using a fluorimeter Fluroskan II (Labsystems, Helsinki Finland). Over time, the fluorescence decreased with photobleaching. By comparison, if the dextran-FITC was kept in the dark and in

the cold, it can remain stable for at least three weeks as seen in Figure 5. The graph shows that over a wide range of concentration, the intensity of the fluorescence does not change if the molecules are refrigerated and kept in the dark.

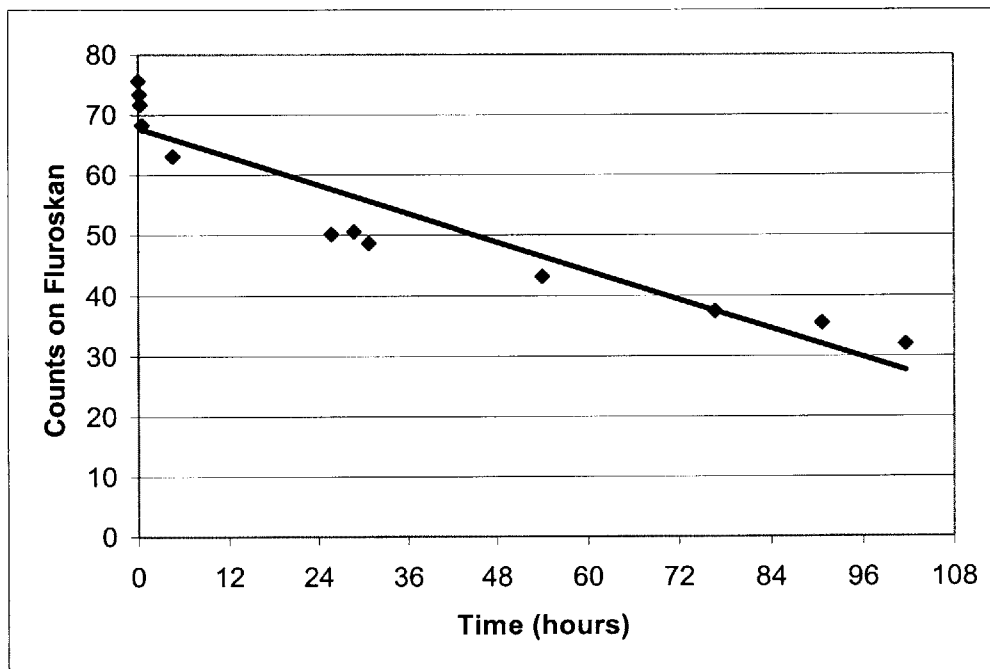


Figure 4: Fluorescence of dextran-FITC degrades upon light exposure. Samples of dextran-FITC fluorescence were taken at various time points as it was exposed to constant room light. Fluorescence remained stable over the first few hours but degraded over time. Its fluorescence intensity was half its initial value after 85 hours.

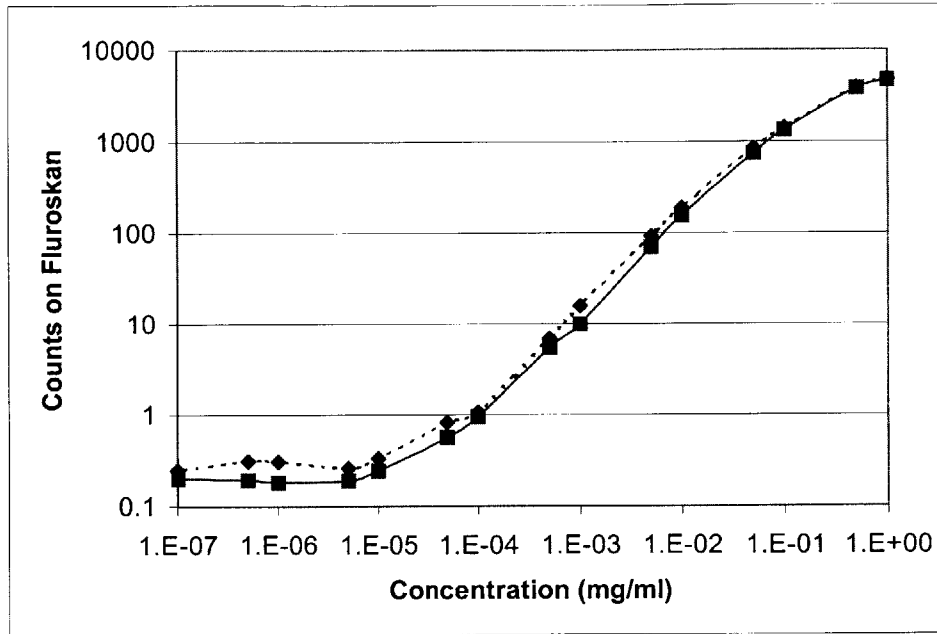


Figure 5: Florescence of dextran-FITC remains stable if refrigerated in the dark. Dextran-FITC of various concentrations were made and its fluorescence tracked over time. The samples were then refrigerated in the dark and its fluorescence taken after three weeks. Initial fluorescence is shown in solid line and fluorescence after three weeks is shown by dotted lines. Graph is a log-log scale.

Chapter 3 FLUOROSCOPY METHOD

3.1 Tissue Preparation and Diffusion Cell

Porcine hearts were obtained from university or hospital animal facilities under NIH and university care guidelines. The hearts were extracted and placed in fresh phosphate buffer saline (PBS⁺⁺) solution with calcium and magnesium to maintain osmotic balance within the tissue. The tissue was transported to the laboratory within three to four hours of extraction and refrigerated until use. The myocardium of the left ventricle was used because it is the thickest part of the heart muscle and probably the most important functional element. It is also the target area of interest for most local drug therapies and interventional treatments. Acquired hearts were then cut and sliced into uniformly thin 1-2 cm sections using a deli meat slicer (Restaurant Supply Corp, Medford, MA). The hearts were cut into two orientations, either to expose the transmural or cross section of the left ventricle. The transmural section exposed the face of the myocardial fiber orientation whereas the cross-section exposed the edges of the muscle fiber sheets. The two orientations are shown in Figure 6. After the tissue was cut into uniformly thin slices, any residual blood was cleaned from inside the ventricle.

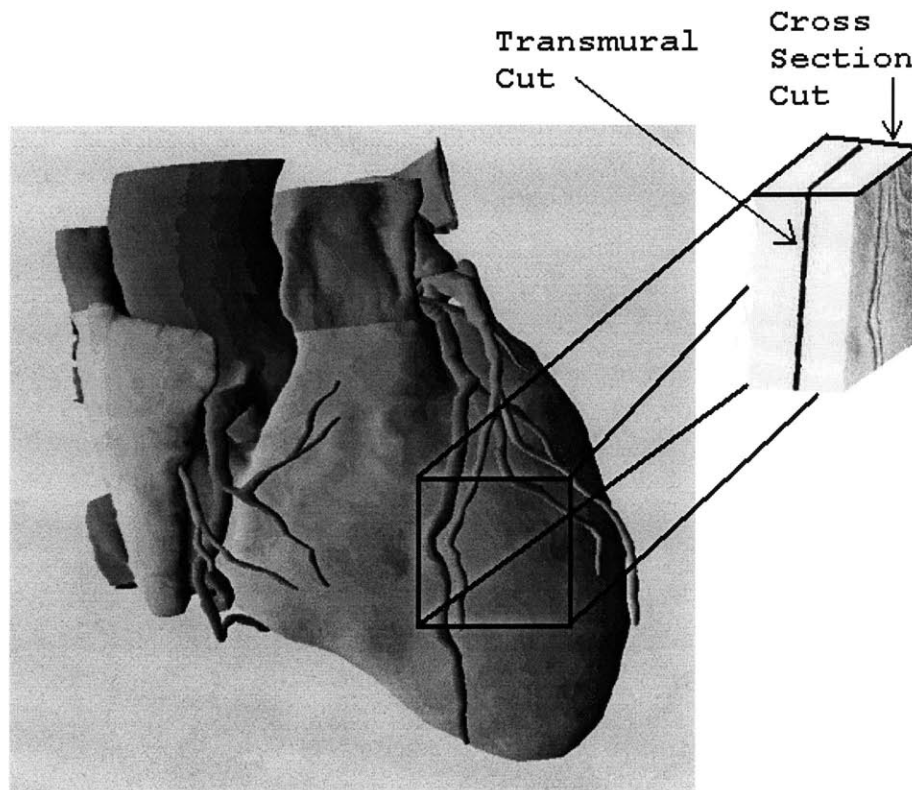


Figure 6: Diagram of the myocardium cutting orientation. Transmural cut exposes the face of the muscle fiber sheets. Cross sectional cut exposes the edge of the muscle fiber sheets. All of the cuts were performed using a commercial grade deli meat slicer. Image from the Digital Anatomist (University of Washington School of Medicine).

After the tissue was sectioned, it was encased in a Franz vertical 3-piece diffusion chamber manufactured by PermeGear (Riegelsville, PA). The three pieces include a top piece for the diffusion source, a bottom piece for the sink and a clamp to tightly seal the tissue between the top and bottom pieces. Figure 7 shows the layout of a diffusion cell with a tissue clamped inside. Orifice size determines the area that the tissue is exposed to the source chamber. Orifice sizes of either 15mm or 20mm in diameter were used. The presence of non-uniform cuts or a large coronary artery at the top surface of the tissue were detected by first using PBS⁺⁺ perfusate to check for leaks out the side. If a leak was found, the section was replaced. Once the system was setup, either 20kDa dextran-FITC (Sigma Chemicals) or 150kDa dextran-FITC in a

concentration of 4 mg/ml was placed in the source chamber. The edges where the tissue was exposed to air were wrapped in parafilm to prevent dehydration. The entire experiment was encased in a dark chamber to prevent photobleaching of the FITC molecule at room temperature. The length of the experiment was approximately four hours.

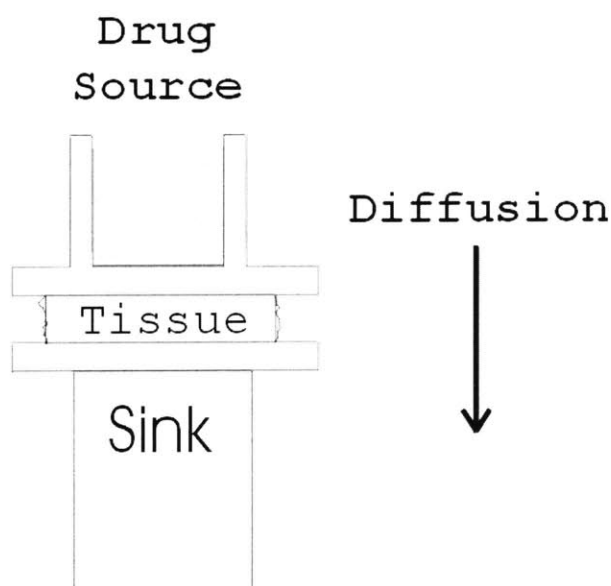


Figure 7: Tissue inside a diffusion cell. An initial concentration of dextran-FITC was placed in the top source chamber to allow for diffusion into the tissue.

With each set of experiments, a standardization tissue concentration curve was made. Separate tubes with small pieces of tissue were incubated in various dilutions of dextran-FITC for 24-48 hours to allow the dextran-FITC bath to equilibrate within the tissue. A standard concentration calibration curve allowed for the conversion of intensities to concentrations.

3.2 Immobilization and Sectioning

At the end of the experiment, the tissues were quickly cut into smaller square pieces and embedding compound immobilized in the tissues by snap freezing which prevented further diffusion. Snap freezing involves placing the tissue in a plastic mold (Polysciences), filling it with embedding medium (OCT, Tissue-Tek), and quickly placing it in a bath of liquid nitrogen

to solidify the medium. The cut tissue sections were placed in the plastic mold in a specific orientation such that the next set of tissue cuts will reveal the distribution profile. The specimen molds with solidified tissue were stored in a dark container at -20° C. The frozen and embedded tissue samples were cut into thin 20µm cross-section slices using a precooled cryostat (Ames Cryostat II, Miles). During the slicing procedure, excess frozen embedding medium was carefully removed to reduce embedding artifact during examination. Tissue slices were put onto glass slides (Superfrost Plus, VWR Scientific) and then freeze-dried in a -50°C lyophilizer (Labconco) for 24 hours in a dark environment. The slides were then stored in 5°C cold room before imaging.

3.3 Image Acquisition System

Images were captured using a CCD video camera system (Optronics) attached to a fluorescence microscope (Optiphot-2, Nikon). The microscope and camera apparatus were mounted on a pneumatic optical table (Technical Manufacturing Corporation) to minimize vibrations, which can introduce noise. Still images were captured using a frame grabber board (LG-3, Scion) connected to a Macintosh compatible computer (Power Computing) using the commercial software package IPLab Spectrum (Signal Analytics). Calibration of the frame grabber board was accomplished by displaying a test image consisting of color bars generated from the video camera system. The gain and offset of the frame were matched to the dynamic range of 0 to 255 units for red, green, and blue channels to the video camera. A 20-fold magnification of the images was obtained with a 10x ocular and 2x objective. The resolution of the images captured was 640 x 480 pixels. A super high pressure mercury lamp (Nikon) provided the light source for the microscope which was allowed to warm up at least two hours prior to use to ensure uniform light output. There were two sets of filters used, UV and FITC.

The UV filter set consisted of an excitation filter of 330-380 nm, a dichroic filter (beamsplitter) of 400nm and a barrier filter of 420 nm. The FITC filter set consisted of an excitation filter of 465-495 nm, a dichroic filter of 505nm and a barrier filter of 515-555nm. The fluorescent tag, FITC, used in the experiment were maximally excited around 490nm so that the UV images contained only autofluorescence and FITC images contained both autofluorescence and signal of interest from the fluorescent labels. All images were taken with both the UV and FITC filter sets and subtracted to remove autofluorescence

3.4 Image Processing

3.4.1 Basic Post-Image Processing

The images were acquired using RGB (red, green, blue) color components and converted to HSV (hue, saturation, value) color model. HSV decouples intensity information away from the color information with hue and saturation representing the color and value representing the intensity. For all of the images, only the value component was saved, which represented the intensity value ranging from 0 (absolute black) to 255 (absolute white), while the hue and saturation values were discarded.

3.4.2 Getting Intensity Profile

All image processing was performed in Matlab v5.3 (Mathworks). First, all the images were examined for tissue cracking or incomplete sectioning. If imperfections were found, the image was removed from further analysis. Next, using a Matlab program, distribution profiles were extracted from the image. To correct for autofluorescence, the UV image was subtracted from the FITC image. To create an average concentration profile, many images and profiles were aggregated. A Matlab program was written to extract concentration profiles from an image. To obtain a set of concentration profiles for each image, a line and a point were defined. Figure

8 labels and shows the steps needed to generate the intensity profiles. The first step was to draw a flat line between two points that corresponded to the edge boundary of the tissue. The edge boundary was defined as the area of tissue where the source concentration was exposed. The second step was to choose a third point that marked the end of the distribution profile. The Matlab program generated a line parallel to the edge boundary line that included the third point. Then a series of intensity distribution profile perpendicular and between the two lines were generated. The same process was performed with the next image for all images in an experiment and then the intensity profiles were combined and averaged to obtain an average intensity distribution profile.

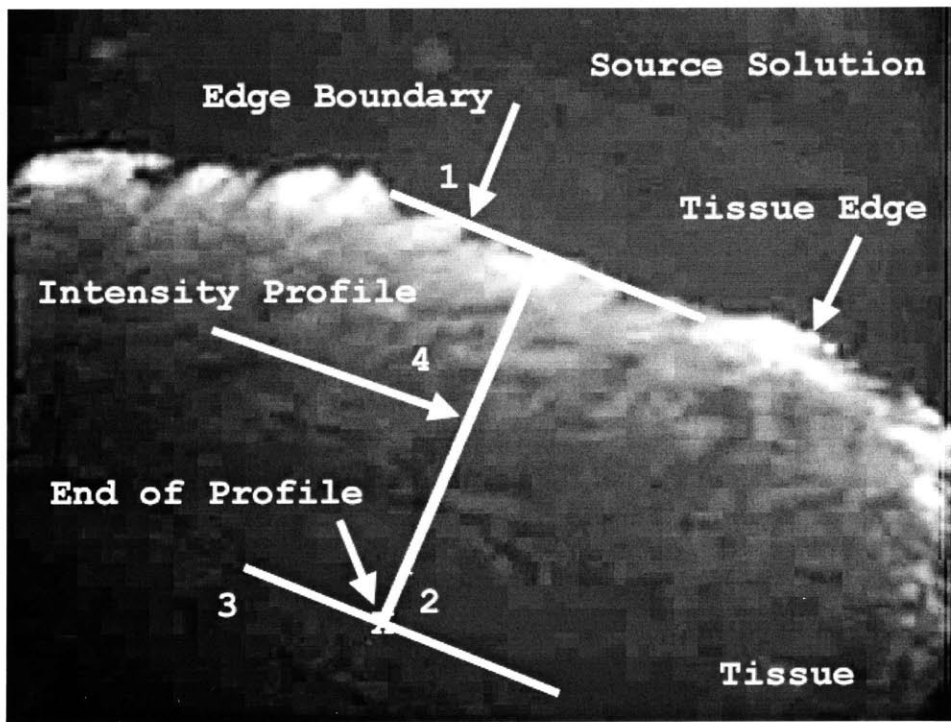


Figure 8: Description of getting intensity distribution profile from an image. The lighter white is the fluorescence of the dextran-FITC. The first step (1) was to define the edge boundary of where the source concentration was exposed. Second, a point (2) that defines the end of the profile was selected. Then the program created a line (3) parallel to the edge boundary and including the end of the profile. Then a series of intensity profiles (4) were generated for this image.

3.4.3 Conversion of Intensity to Concentration

The intensity distribution profile generated above was an intensity value versus distance from the edge of the tissue. To convert to concentration, a separate intensity to concentration standard curve needed to be created for each experiment run. The reason for this was that fluorescent microscopy is usually considered a binary tool to determine the presence or non-presence of a compound. Quantitative measurements of fluorescent markers are not particularly accurate since intensity of fluorescence may change from time to time. To make it quantitative, a standard intensity to concentration curve needs to be developed each time. To create a standard curve, small samples of tissue were incubated in various concentrations of dextran-FITC of a specific molecular weight for 24 to 48 hours. The tissue was snap frozen and cut into 20 μ m thin slices using the Cryostat. A digital intensity image was taken as described above. If the tissue equilibrated with the dextran-FITC, the tissue intensity value was relatively uniform. A small region of the tissue was selected to get an average intensity value that corresponded to the bulk fluid concentration the tissue was incubated in. The same process was repeated for each tissue incubated at various dextran-FITC concentrations. A linear relationship between intensity and bulk fluid concentration was determined and used to calculate bulk fluid concentration from intensity.

To convert bulk fluid concentration to tissue concentration, fractional free space, ϵ , must be calculated. Fractional free space represents the amount of dextran-FITC that can maximally diffuse into the tissue. This value ranges from 0 to 1 and is calculated for each dextran-FITC molecular weight and has the units of ml of bulk fluid /ml of tissue. To measure fractional free space, a small piece of tissue was weighed and placed into a known concentration of a compound solution for a few days to equilibrate. The tissue was then removed and cleaned of excess

solution from the surface and placed into fresh PBS⁺⁺ to elude out the compound from within the tissue. The amount of compound that eluded out of the tissue was then used to calculate the fractional free space.

After completing all the image processing steps, a quantitative concentration profiles from the tissue was extracted. Once the concentration profile and distribution were known, diffusion parameters were calculated by fitting simple diffusion models.

Chapter 4 DIFFUSION MODEL

4.1 Mechanism of Transport

In a living tissue, the transport of a macromolecule can be affected by many mechanisms that may not be easy to separate into individual components. To understand the mechanism of transport, it is important to first recognize the various mechanisms that can contribute and then try to isolate each of them to study. A brief summary of possible mechanisms of transport mechanisms in the heart will be discussed.

The first and most basic transport property is diffusion. Diffusion is the movement of macromolecules driven by random molecular motions and can usually be described as transport through a concentration gradient from high to low. Basic equations based on Fick's first and second law of diffusion and the continuity equation describe the diffusion of molecules. A simple diffusion equation can be written by using all three equations (Equation 4.1). C is the concentration of the macromolecule in the tissue (number of macromolecule / volume of tissue). D is the diffusivity or diffusion coefficient in (nm^2/s). ∇C is the gradient of the concentration. Equation 4.1 describes how concentration changes over time depending on D and the gradient square of concentration. If the transport of the macromolecule is isotropic, then D will be the same in all directions. However, if the transport is non-isotropic, then there will be a separate D for each direction.

$$\frac{\partial C}{\partial t} = D \nabla^2 C \quad (4.1)$$

Convection is described as the movement of molecules with bulk fluid flow. In the living system, convection is established by a difference in pressure from one side to another, causing fluid flow to move in one direction. Equation 4.2 describes the contribution of convection to transport. V is the velocity of bulk fluid flow (nm/s). Convection can be seen in the myocardium where there is a pressure gradient from inside the ventricles, at the endocardium, to the outside of the heart, epicardium. The pressure gradient forces bulk fluid to flow from the endocardium to the epicardium.

$$\frac{\partial C}{\partial t} = -V\nabla C \quad (4.2)$$

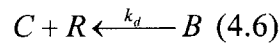
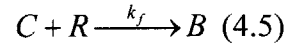
Electrodiffusion may also play a role in the heart. Electrodiffusion is the movement of charged particles through an electrical potential gradient. Equation 4.3 describes the contribution of electrodiffusion to transport. U is the mobility of the macromolecule. Z is the valence/charge of the macromolecule. F is Faraday's constant, $9.65E4$ Coulombs/mol. E is the electric potential gradient (V/m). Mobility can be calculated from the diffusivity from the Einstein relation shown in Equation 4.4. Q is the electrical charge, k is the Boltzman constant and T is temperature in Kelvin. The heart, with its electrical conducting system, generates an electric field inside the heart that may affect the movement of charged particles.

$$\frac{\partial C}{\partial t} = -uzFE\nabla C \quad (4.3)$$

$$\frac{u}{D} = \frac{q}{kT} \quad (4.4)$$

Binding and unbinding of molecules to receptors on cells, as well as the consumption and generation of molecules in the cell may also affect macromolecular transport. Many proteins and compounds within living tissue bind to receptors on cells, and affect the transport of molecules through the tissue. The consumption and generation of molecules in cells can also affect the

effective transport of molecule inside the tissue. Simple binding kinetics are shown in equations 4.5 and 4.6. R is the concentration of the receptors, and B is the concentration of the bound molecule and receptor. k_f and k_d are the rate constants of the forward and backward reaction. Equation 4.7 shows the contribution of binding and unbinding and consumption and generation in transport. G and X are the generation rate and consumption rate of the compound by the cells.



$$\frac{\partial C}{\partial t} = -k_f CR + k_d B - X + G \quad (4.7)$$

Equation 4.8 combines all of the transport mechanisms into one single equation.

$$\frac{\partial C}{\partial t} = D\nabla^2 C - V\nabla C - uzFE\nabla C - k_f CR + k_d B - X + G \quad (4.8)$$

With all of these forces actively playing a part in transport in the heart, it is difficult to isolate the contribution of each individual component. Ideally, experiments should be designed to change only one parameter at a time, while keeping the others constant or eliminated entirely. The isolation of individual components may be impossible in *in vivo* systems, but may well be possible *ex vivo*.

4.2 Modeling Transport

Mathematical modeling of transport was done using Matlab. The forward-difference analysis on solving partial differential equations was used and the Crank-Nicolson solution method employed. One can model a concentration profile given diffusion parameters, initial concentration bath, and time of experiment. Experiment data were then fit to a simulation model. A simple model of single directional diffusion was used. This was a valid assumption

because the distance traveled into the tissue relative to the total surface area of compound contact was small. This simplified the transport equation from 4.8 to 4.9.

$$\frac{\partial C(x,t)}{\partial t} = D \frac{\partial^2 C(x,t)}{\partial x^2} \quad (4.9)$$

$C(x,t)$ is a linear concentration distribution profile of the molecule of interest as a function of distance and time. D is the diffusivity and is expressed in $\mu\text{m}^2/\text{sec}$. This is a much more simple differential equation to solve. If the concentration profile is known, the diffusion coefficient, D , can be calculated.

4.3 Simulating PDE Using Crank-Nicolson Method

The basic method to numerically solving differential equations is to use the finite difference equation. Ordinary differential equations are usually straightforward and easy to solve. But partial differential equations (PDE) are more difficult to solve and explicit solutions are not easily found. The diffusion equation is a partial differential equation with partial derivatives to both distance and time. Answers to partial differential equations are usually found by numerical methods.

An inherent complication in numerically solving difference equations is the possibility of generating unstable solutions. Instability generally arises when the step sizes in the difference equations are too large and when round off errors in each step are no longer insignificant. Through mathematical proof, instability usually occurs when the step size ratio $r = dt/(dC)^2$ is less than $\frac{1}{2}$ where t is time and C is concentration. If the step sizes are too large, the solutions, which are iteratively computed, can sometimes lead to wildly oscillatory diverging numbers.

Partial differential equations often are of the form:

$$au_{xx} + 2bu_{xy} + cu_{yy} = F(x, y, u, u_x, u_y)$$

Numerically solving partial differential equations requires first classifying the type of partial differential equation. The three subclassifications are:

PDE Type	Criteria	Typical Equations
Elliptic Type	$ac - b^2 > 0$	Laplace equation
Parabolic Type	$ac - b^2 = 0$	Heat equation
Hyperbolic Type	$ac - b^2 < 0$	Wave equation

Diffusion equation is classified as parabolic and a numeric solution method for parabolic equations was used. A widely used numeric solution method is the Crank Nicolson method proposed in 1947. Its main advantage is its ability to generate stable answers even when $r > 1/2$. This allowed for selecting larger step sizes and reduced the number of calculations needed. The Crank Nicolson method replaces the d^2C/dx^2 term by the mean of its finite-difference representations on the t^{th} and $(t+1)^{\text{th}}$ time row where t is time and $t+1$ is the next time step (Crank 1975, Kreyszig 1993). The result is the creation of a set of simultaneous equations for each time step. The set of simultaneous equations form a matrix and can be easily solved using Matlab. Solving the set of simultaneous equations results in finding each point in time implicitly, also known as the implicit method. The solution matrix is the concentration profile at each point for all time steps.

Mathematical modeling of transport had been done extensively in the past on transvascular transport and gaseous transport through tissue. This thesis was one of the first attempts to try and quantify transport of a compound through myocardial tissue. Once a concentration profile from the experiment was obtained, its profile was used in the mathematical model to calculate a diffusivity number that produced a simulated concentration profile that most closely matched experimental data.

Chapter 5 QUANTIFICATION OF MYOCARDIAL MACROMOLECULAR TRANSPORT

5.1 Introduction

Myocardial molecular transport is increasingly receiving attention because of its potential for elucidating mechanisms and providing therapies for the most prevalent and morbid of all diseases. This is important because of the fact that heart disease is the leading cause of morbidity and mortality in the United States, and there are currently an absence of good therapies for it. Many have tried to prevent restenosis or stimulate angiogenesis by delivering heparin to coronaries and growth factors like FGF-2 to the heart. The most promising solutions are those that involve local drug delivery. However, as described previously, most research work in this area has focused on the end effects and not at the mechanisms or distribution of the compound in the tissue. The ability to quantitatively assess the distribution of macromolecules in the heart can be important in assessing the strengths or shortcomings of a drug delivery device design. The goal of this thesis was to develop a better technique for quantification of myocardial macromolecular transport.

For this research project, fluorescence microscopy was modified and extended to look at distribution and transport of macromolecules in myocardial tissue. It was demonstrated that quantitative distribution profiles of transport could be accomplished in the myocardial tissue. Quantitative distribution profiles were used to look at simple diffusion of dextrans tagged with fluorescent FITC in the myocardium. Attractive properties of dextrans included being widely available, do not bind to cells, are stable, can be cross-linked to various sizes, and easily

modified chemically. Diffusion of dextrans in myocardium was evaluated in two directions, transmural and cross-sectional. Transmural transport is the movement of macromolecules directly from the inner ventricles to the outside of the heart in face of the myocardial fiber sheets. Cross-sectional transport is the movement of macromolecules in the direction of the apex of the heart to the outlets of the heart or between the myocardial fiber sheets. *Ex vivo* experiments were performed to look only at diffusion and to remove the effects of convection, electrodiffusion and other complications from a live beating heart. This gave a good first estimate of pure diffusion in the myocardium.

5.2 Materials and Methods

5.2.1 Tissue Preparation and Diffusion Cell

Porcine hearts were obtained and prepared as specified in Chapter 3.1. The porcine heart after arrival from the animal facility was quickly cleaned and prepared for diffusional studies. The heart was then cut into uniformly thin 1-2 cm slices using a deli meat slicer to produce a flat and unfrayed edge of the myocardium. The ability to cut the myocardium into a uniformly flat surface allowed diffusion to be modeled as a large flat surface and to remove edge effects since the area of the surface was much greater than the depth of penetration. The edge of the myocardium could be examined histologically after all tissue processing without drug application to check for a flat edge surface for diffusion. After the tissue was cut into thin 20um profile slices from the Cryostat, the tissue was cleaned of OCT and stained with hematoxylin and eosin (H&E) to look at the histology of the myocardium.

Figure 9 shows that the tissue could be prepared with a clean and flat surface for examination of drug diffusion. Figure 10 shows a higher magnification of the myocardium. Individual cardiac nuclei are stained in blue, and definite muscle orientation can be seen, going

left to right in this image. The lack of heavy pink stains meant that there was not much cytoplasm in the cell nor a lot of collagen. The tissue can be traumatized in processing that involves repeated cutting and freezing, and artifacts might form such as the hole on the right hand side in Figure 9. Whenever images showed tissues artifact, profiles of macromolecular transport were not taken from that area.

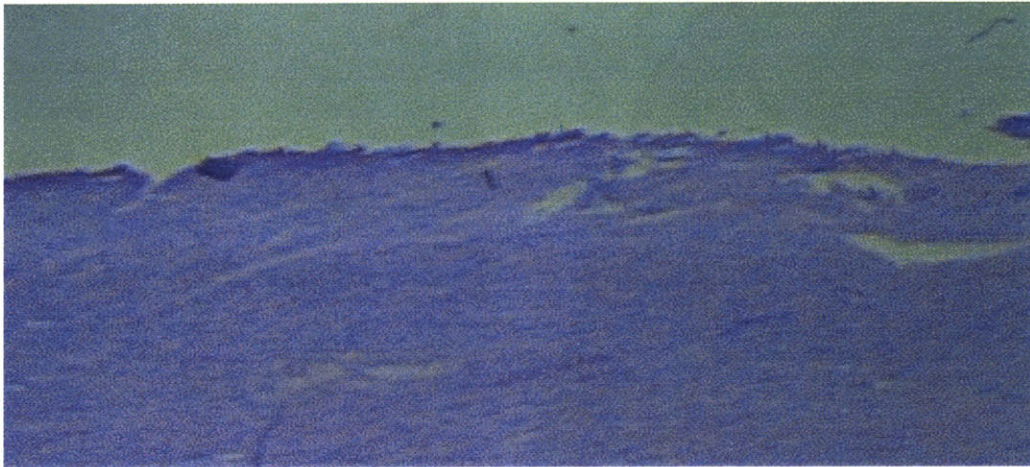


Figure 9: H&E stain of porcine myocardium. The top surface is cut to produce a flat surface where the drug source was exposed. Tissue separation on the right surface is an artifact of tissue processing. Picture taken at 20X.

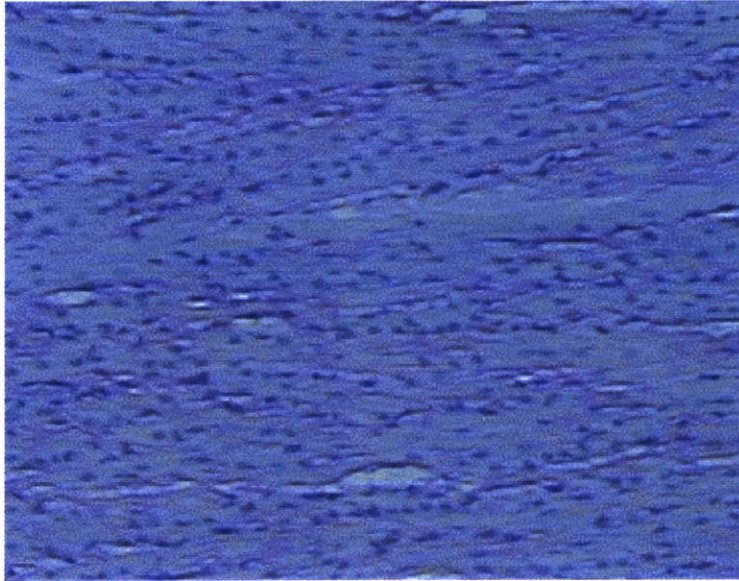


Figure 10: High power magnification H&E stain of porcine myocardium. Cardiac fibers can be seen having a uniform orientation and direction. The cardiac nuclei are clearly seen as dark blue spots. Cytoplasm, collagen, and other structures are seen in pink. Picture taken at 100X.

After the tissue was cleaned and cut into small sections, a small piece was placed and clamped into a diffusion cell chamber (Figure 7). Dextran-FITC was placed in the source chamber and was allowed to diffuse into the myocardium for approximately four hours. A concentration of 4mg/ml of both 20kDa and 150kDa molecular weights dextran-FITC were used to compare the transport property of macromolecules of different sizes. Since growth factors are about 20kDa in size, the 20kDa dextran can be a model for transport of these macromolecules. The 150kDa dextran might model transport of larger macromolecules. Since the size of the source chamber was relatively large, it was assumed that the concentration of the source chamber did not change over time. This was verified by comparing fluorometric determination of the intensity of dextran-FITC samples from the source chamber before and after the experiment to insure that the fluorescence had not changed during the entire duration of the experiment.

Along with the experiment, a standard tissue concentration for each dextran molecular weight was made. Additional small pieces of tissue were cut and placed in a small 10ml vials

filled with dextran-FITC at different concentrations. The tissue was refrigerated and kept in the dark for 24- 48 hours to allow the bulk solution to equilibrate within the tissue.

5.2.2 Immobilization and Sectioning and Image Acquisition

At the end of the experiment, the tissue was removed from the source and cleaned of excess dextran-FITC that may still have been on the surface and snap frozen as described in section 3.2. The freezing of tissue stopped and prevented any further diffusion. The frozen tissues were then stored in -20°C freezer until they were cut into thinner slices using the Cryostat. The tissue incubated in the standard concentration dilutions were also snap frozen after they equilibrated with the tissue and then sliced into $20\mu\text{m}$ thin slices using the Cryostat. After the tissues were cut into thin $20\mu\text{m}$ slices, mounted on a glass slide and lyophilized dry, digital images were taken. The image acquisition system is described in detail in section 3.3. Digital fluorescent images were captured and stored on the computer for data analysis later.

5.2.3 Image Analysis

5.2.3.1 Basic Post-Image Processing

The fluorescent image acquired was a greenish RGB image as the FITC fluoresces at the green wavelength. The RGB image was converted to HSV and only the intensity value decoupled from the color data saved. Figure 11 shows the image in RGB and after the intensity value was spliced out. A concentration profile gradient can be easily seen. The drug source was presented at the top surface and diffused down into the tissue. A flat edge can be seen demarcating the edge of the myocardium.

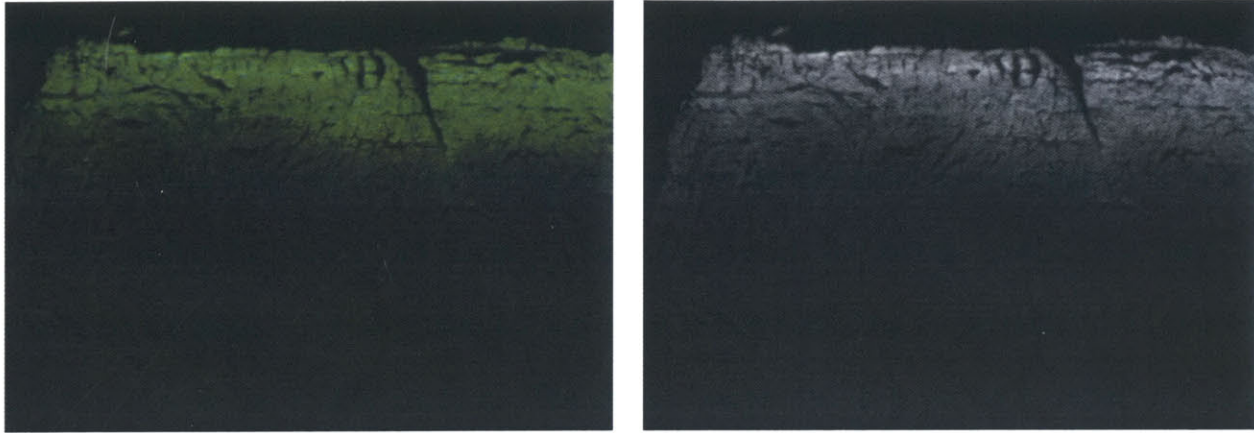


Figure 11: FITC Fluorescent image (left) and its intensity image (right) of the myocardium. The drug source was presented at the top and it diffused down into the tissue. A concentration profile gradient can be seen.

5.2.3.2 *Acquiring Intensity Profile*

After the intensity values of the images were extracted, they were imported and read into Matlab for data and image analysis. A Matlab program cycled through all of the images and allowed for definition of the border and end profile. Detailed description of program performance is described in 3.4.2 and the Matlab code is located in the appendix. Figure 12(a) shows an example of the intensity distribution profile obtained from numerous image and individual profiles. The small dots were a set of profiles and the thick line was the average of all the profiles. The average profile was the mean of approximately 2000 profiles. For most profiles, the intensity distribution could be observed to rise initially before declining. This was because the definition edge boundary was slightly above the true edge. The edge boundary of the tissue where drug begins to diffuse was defined to be the first point from the beginning of the average profile that had a zero slope. The derivative of the average profile was used to determine the slope. The slope was initially positive corresponding to the initial rise before it becomes zero as the profile plateaus. The average curve was then shifted to reflect the new

boundary. This is seen in Figure 12(b) where the graph is shifted over by 10 points to get the edge boundary.

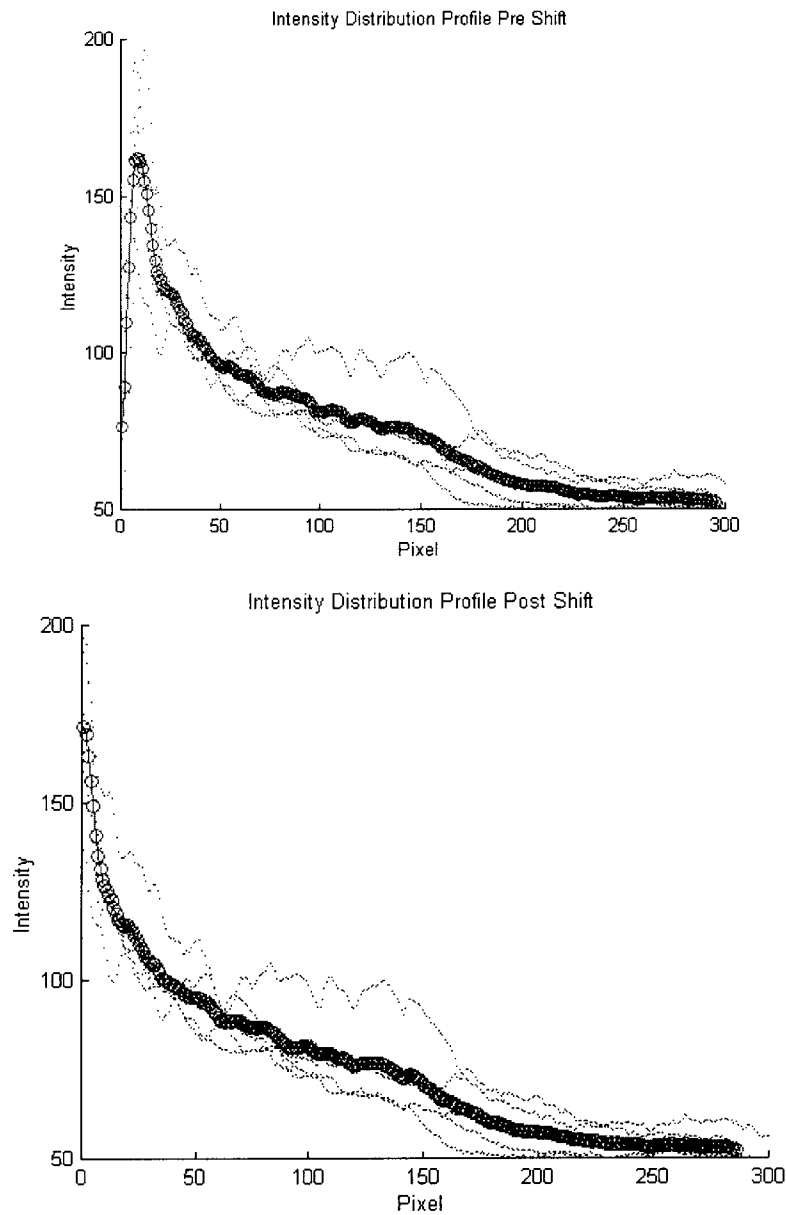


Figure 12: Intensity distribution profile pre and post shift. The small dotted lines are sets of profiles from an image and the thick circle line is the average of all the profiles. This average contained 1641 individual profiles. (a) Top graph shows the intensity distribution profile from numerous images. Defining the edge of the boundary above the true edge caused the initial upward slope. (b) Bottom graph shows the shifted intensity distribution profile to define the true edge of the myocardium. A total of 10 points were removed from (a) to (b).

5.2.3.3 Conversion of Intensity to Concentration

After the intensity distribution profile was created, the intensity was converted to tissue concentration using a standard intensity to bulk solution concentration curve derived for each use. For each standard tissue image, a rectangular area in the middle of the tissue was used to calculate the average intensity for a certain bulk fluid concentration. A best fit linear relationship was determined from the intensity vs. bulk concentration graph. One relationship is shown in Figure 13 and summarized with its equations in Table 2.

Dextran-FITC Size	Average Mol Weight	Concentration Equation (mg / ml fluid)
20KD	19500	$Conc = \frac{(Intensity - 37.53)}{40.93}$
150KD	148000	$Conc = \frac{(Intensity - 58.38)}{19.92}$

Table 2: Bulk fluid concentration from intensity equation. The equation is derived from the best-fit line of the plot shown in Figure 13. This equation was used for one set of experiments when a set of fluorescent images was taken at one sitting.

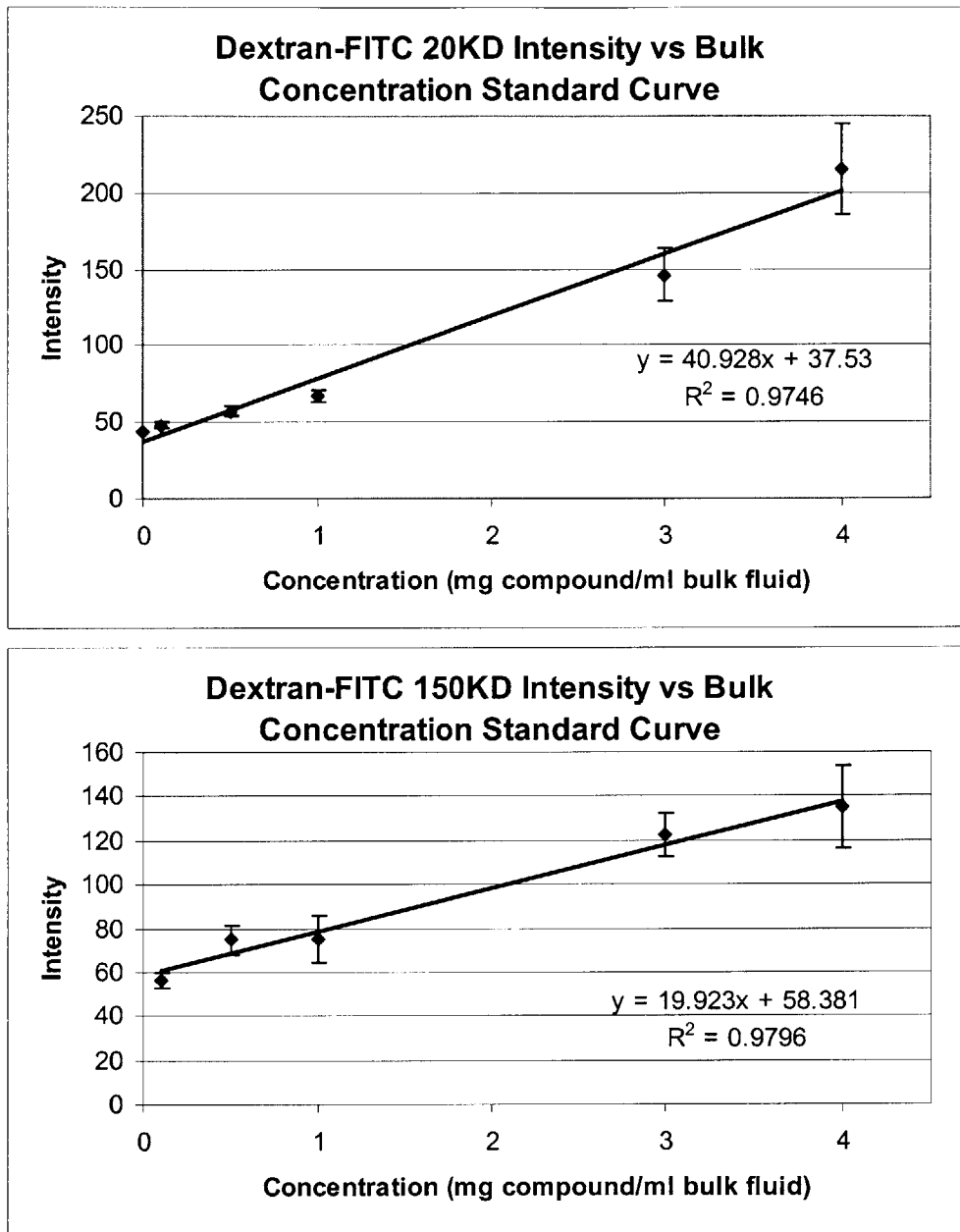


Figure 13: Intensity to Concentration Standard Curve. (Top) 20KD Dextran-FITC (Bottom) 150KD Dextran-FITC.

Tissue volume was determined from bulk fluid volume through the knowledge of the free fractional space (ϵ) of each molecular weight in tissue (Section 3.4.3 and Table 3). One final conversion from mg of compound to number of compound particles was performed using the average molecular weight.

Dextran-FITC Size	Free Fractional Space (ϵ) $\frac{ml(bulk_fluid)}{ml(tissue)}$	Standard Deviation
20KD	0.454	0.065
150KD	0.261	0.020

Table 3: Free fractional space (ϵ) of dextran-FITC in myocardium.

5.2.3.4 Calculation of Diffusivity

After quantitative tissue concentration profiles were calculated, the curve was fit to a simple diffusion model written in Matlab. The program used a Nelder-Mead function-minimization routine to solve for diffusion parameters using a mean-square error between the experimental and simulated concentration profiles. Since the length of the profile was determined by the number of pixels, the simulation only needed to simulate diffusion to a certain distance to reduce the number of calculations. With the 2X objective resulting in 20X magnification, each mm was about 151 pixels. The length of the simulated diffusion was broken up into smaller nodes. If every pixel was to become a node, the number of calculations would be enormous and the simulation would be prohibitively slow. To reduce computation time, 40 nodes were defined across the entire simulated length. Initial boundary conditions and an estimate of diffusivity were used to initiate the model. Figure 14 shows an experimental concentration profile and its best fit concentration profile by varying D, diffusivity, given the initial boundary conditions.

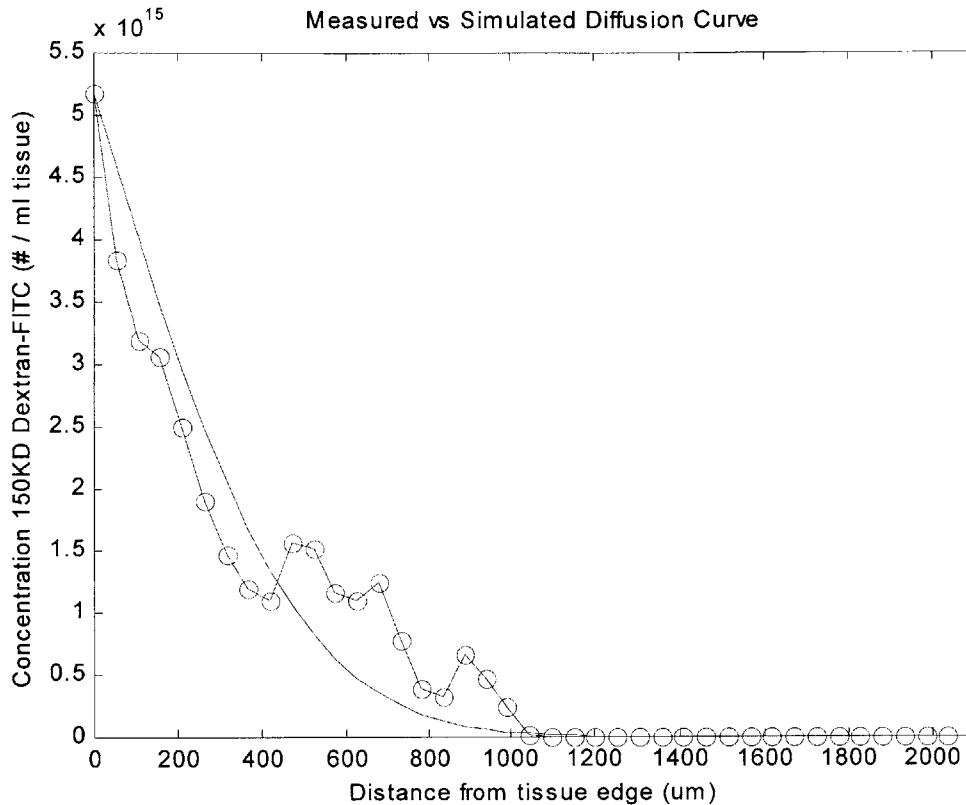


Figure 14: Concentration profile of measured versus simulated. The measured concentration profile (line with o) as compared to the best fit simulated diffusion curve (solid line).
 $D = 4.43 \mu\text{m}^2/\text{s}$.

5.3 Results

N=3	Diffusivity ($\mu\text{m}^2/\text{s}$)	Standard Dev
20KD Transmural	9.49	2.71
20KD Cross-Section	20.12	4.10
150KD Transmural	2.39	1.86
150KD Cross-Section	3.23	1.76

Table 4: Summary of the diffusivity of dextran-FITC in porcine myocardium. Using the diffusion model to fit the measure concentration profile, a diffusivity number was calculated.

Table 4 summarizes the results of diffusivities found by the simulation program to best fit a concentration profile to the experimental concentration profile. The diffusivity of the 20kDa was 3.9 fold faster than the 150kDa in the transmural direction ($9.49\mu\text{m}^2/\text{s}$ vs. $2.39\mu\text{m}^2/\text{s}$ $p < 0.02$), and 6.22 fold faster in the cross-sectional direction ($20.12\mu\text{m}^2/\text{s}$ vs. $3.23\mu\text{m}^2/\text{s}$ $p < 0.01$).

Diffusion in the cross-sectional direction was statistically different than in the transmural direction for the 20kDa dextran ($20.12\mu\text{m}^2/\text{s}$ vs. $9.49\mu\text{m}^2/\text{s}$ $p < 0.03$) but not for the 150kDa ($3.23\mu\text{m}^2/\text{s}$ vs. $2.39\mu\text{m}^2/\text{s}$ $p < 0.59$).

Comparison between diffusivity in the myocardium and in the arteries might be made since they are both derived from similar sources embryologically. Previously published diffusivity numbers look at transport of dextrans in the transmural direction from outside to inside the arteries (Elmalak et al 2000). Table 5 summarizes the diffusivities of dextran-FITC found in arteries and compares them with the diffusivities calculated for myocardium.

Dextran Size	Previously Published D ($\mu\text{m}^2/\text{s}$) In rat artery	Calculated D ($\mu\text{m}^2/\text{s}$) In porcine myocardium
10kDa	9.33±0.76	
20kDa		9.49±2.71
38kDa	8.21±0.71	
78kDa	4.79±1.55	
150kDa		2.39±1.86
282kDa	2.26±0.65	

Table 5: Summary of dextran diffusivities from previous studies compared to values in the myocardium. The diffusivities of similar molecular weights have similar diffusivities in the myocardium and arterial wall.

5.4 Discussion

Using the method developed and described here, it was possible to look quantitatively at macromolecular transport through tissue. This will be important in defining the distribution and transport of various compounds in the heart. Smaller molecular weight compounds diffused much faster than those of larger molecular weight, as expected. This result can be expected since the smaller dextran can better maneuver between the cells and tightly packed muscle fibers more easily than the larger dextrans. For the small dextran, there was a significant difference in the diffusivities in the two directions whereas no significance was found for the larger dextran. This may be explained by muscle fiber orientation and presence of fascial planes. Cardiac muscle are

tightly packed to form a strongly-netted vertical sheet wrapping capable of providing elasticity for filling of the heart and forceful contractility for ejection of blood. Separating the cardiac muscle fiber sheets are fascial planes which allow the muscle sheets to easily slide over one another. Transport in the transmural direction must cross the muscle sheets and fascial planes and both might serve as barriers to the movement of molecules. However, transport in the cross-sectional direction, does not move against the muscle sheets or fascial plane, but rather in between them. The difference in transport in the two directions of the small macromolecule suggest that there is less hindrance of the smaller molecule in the cross-sectional direction indicating that the smaller molecules can more easily transport between muscle and fascial sheets. But the larger macromolecule seems to be hindered in both directions equally.

From Table 5, it seems that the similarities in calculated diffusivity of dextrans in the rat carotid arteries and myocardium allow us to return to the question as whether the heart is just a big artery. It seems that the heart myocardium may have similar transport properties to that of an artery in the transmural direction. This can be explained embryologically by that both the myocardium and tunica media are derived from the same embryonic cell types and the fact that both are muscle cells in wrapped in a similar direction.

Chapter 6 CONCLUSION

6.1 Accomplishments

There had been no good method to quantify macromolecular transport in tissue and no attempt to examine these issues in the myocardial tissue. With current techniques being limited by post-experiment artifact, low signal-to-noise and poor spatial resolution, new and better methods needed to be developed. Novel and more quantitative methods will be beneficial in the study of drug transport. With the movement of these therapeutic innovation towards local drug delivery, a new and quantitative method is needed to examine the distribution of macromolecular transport. Since the delivery is targeted to a specific area, being able to study the transport mechanism locally becomes even more important. In this thesis work, a technique was extended and further developed to look at macromolecular transport. This technique was applied to look at simple diffusion of a representative macromolecule, dextran, in the porcine myocardium tissue. The diffusion of fluorescent labeled dextran was examined in two directions *ex vivo* to isolate diffusion and to remove other mechanisms of transport. A quantifiable concentration profile was extracted and fit to a simple mathematical diffusion model to determine diffusivity.

The results of the diffusivity calculations showed that the smaller macromolecules' diffusion coefficient was larger than the larger macromolecule both in the transmural and cross-section direction. The results also showed that only the smaller macromolecule's diffusion coefficient was different in the two directions but was statistically the same for the larger macromolecule. A final result showed that the transport of macromolecules in the transmural

direction may be similar to that of an artery media as the diffusivity numbers were similar between the two for the macromolecular size when compared to previously published numbers.

6.2 Future Work

This thesis extended a system to examine macromolecular transport as a promising technique for looking at and understanding the transport mechanisms of macromolecules in tissue. There are many potential uses for this technique as research in the past has not been able to look quantitatively at the distribution of macromolecules. As with all new techniques, this method needs to be further developed and more thoroughly tested. A natural extension would be to examine more sizes of macromolecules to narrow down the point at which the diffusion in the two directions converge, and if diffusion in myocardium and blood vessels diverge. Many sizes of dextrans-FITC can be easily purchased to use.

In this thesis, only two directions were examined since they were the most important. The third direction would be the direction of moving from side to side of the myocardial muscle. This would approximate the movement of macromolecules along the length of the muscle fibers. It would be interesting how the diffusion coefficient of the third direction compared to the other two directions. This would give insight into which direction diffusion occurs the fastest or slowest and can be used as a guide for delivering drugs locally.

A natural extension to this technique would be to look at specific compounds. One possibility that has been brought up is to examine FGF-2 in the myocardial tissue. Significant research and clinical work have tried to understand how growth factors might induce angiogenesis in myocardial tissue. However little work has been done to look at the distribution of these growth factors once it has been delivered into the myocardium either systemically or

locally. This technique may be extremely helpful in determining the extent of macromolecular transport.

Appendix A: SIMULATING THE DIFFUSION EQUATION USING CRANK-NICOLSON METHOD

The derivation begins with looking at Fick's first law of diffusion (A.1) which says that the flux of particles Φ (mol/nm²s) in the x direction is proportional to the spatial gradient of particle concentration and diffusivity D (nm²/s). The continuity equation (A.2) states that the movement of particles in and out of an area is equal to the change in the concentration of the area over time. By rewriting the flux term as the difference of the flux in and flux out, A.2 become A.3.

$$\Phi(x,t) = -D \frac{\partial C(x,t)}{\partial x} \quad (\text{A.1})$$

$$\frac{\partial \Phi(x,t)}{\partial x} = -\frac{\partial C(x,t)}{\partial t} \quad (\text{A.2})$$

$$\Phi_{in} - \Phi_{out} = \frac{\Delta C}{\Delta t} \Delta x \quad (\text{A.3})$$

Assume that the diffusion length is broken down into n smaller nodes and concentration at each node and at each time step can be defined. Then A.1 describing the flux of particles can be rewritten as A.4. A.3 and A.4 can be combined and rearranged to become A.5 which is the difference equation form of the diffusion equation. Since the Crank-Nicolson method assumes a mean average of two time steps, the left side of A.5 is rewritten to A.6.

$$\Phi = D \frac{C_{n+1}^t - C_n^t}{\Delta x} \quad (\text{A.4})$$

$$D \left(\frac{C_{n-1}^t - 2C_n^t + C_{n+1}^t}{\Delta x^2} \right) = \frac{C_n^{t+1} - C_n^t}{\Delta t} \quad (\text{A.5})$$

$$\frac{D\Delta t}{\Delta x^2} \left(\frac{C_{n-1}^{t+1} - 2C_n^{t+1} + C_{n+1}^{t+1}}{2} + \frac{C_{n-1}^t - 2C_n^t + C_{n+1}^t}{2} \right) = C_n^{t+1} - C_n^t \quad (\text{A.6})$$

Then the terms are rearranged to isolate the different time terms to each side (A.7) where

$G = \frac{D\Delta t}{\Delta x^2}$. Each time step will result in a similar equation similar to A.7. One can see that these

simultaneous equations form a matrix (A.8) where the number of columns corresponds to the

number of nodes and the number of rows corresponds to the number of time steps.

$$-\frac{G}{2}C_{n-1}^{t+1} + (1+G)C_n^{t+1} - \frac{G}{2}C_{n+1}^{t+1} = \frac{G}{2}C_{n-1}^t + (1-G)C_n^t + \frac{G}{2}C_{n+1}^t \quad (\text{A.7})$$

$$\begin{bmatrix} 1+G & -\frac{G}{2} & 0 & 0 & 0 & 0 & \dots \\ -\frac{G}{2} & 1+G & -\frac{G}{2} & 0 & 0 & 0 & \dots \\ 0 & -\frac{G}{2} & 1+G & -\frac{G}{2} & 0 & 0 & \dots \\ \dots & \dots & \dots & \dots & -\frac{G}{2} & 1+G & -\frac{G}{2} \end{bmatrix} \begin{bmatrix} C_0^{t+1} \\ C_1^{t+1} \\ \dots \\ C_n^{t+1} \end{bmatrix} = \begin{bmatrix} 1-G & \frac{G}{2} & 0 & 0 & 0 & 0 & \dots \\ \frac{G}{2} & 1-G & \frac{G}{2} & 0 & 0 & 0 & \dots \\ 0 & \frac{G}{2} & 1-G & \frac{G}{2} & 0 & 0 & \dots \\ \dots & \dots & \dots & \dots & \frac{G}{2} & 1-G & \frac{G}{2} \end{bmatrix} \begin{bmatrix} C_0^t \\ C_1^t \\ \dots \\ C_n^t \end{bmatrix} \quad (\text{A.8})$$

The initial concentration is just an additional vector added to the right hand side of equation A.8

since the source is a constant source. The matrix can be solved to get concentration at each node

and at each time point for a specific diffusivity given the initial concentration.

Appendix B: EXPERIMENTAL DATA

Time (Hrs)	Tissue Concentration (mg/ml)			Average	Standard Deviation
	Tissue #1	Tissue #2	Tissue #2		
0.00	75.99	76.44	76.77	75.65	1.54
0.17	75.72	72.62	71.97	73.44	2.00
0.28	72.43	71.97	70.76	71.72	0.86
0.53	69.39	69.09	66.50	68.33	1.59
4.58	62.60	61.78	64.98	63.12	1.66
25.72	51.42	50.08	48.91	50.14	1.26
28.72	50.94	50.34	50.30	50.53	0.36
30.72	49.21	47.95	48.95	48.70	0.67
54.00	43.37	43.08	43.06	43.17	0.17
76.78	37.55	37.97	36.80	37.44	0.59
90.70	35.36	35.36	35.58	35.43	0.13
101.65	31.99	32.34	31.66	32.00	0.34

Table 6: Experimental data for Figure 4

Concentration (mg/ml)	Tissue #1 Count	Tissue #2 Count	Tissue #3 Count	Average Count	Standard Deviation	Average 3 Weeks Later	Standard Deviation 3 weeks later
1	4766	4678	4694	4712.67	46.88	4643.67	47.54
0.5	3827	3845	3860	3844.00	16.52	3768.67	14.22
0.1	1364	1438	1404	1402.00	37.04	1328.33	18.93
5.00E-02	859.6	841.9	841.8	847.77	10.25	752.40	13.26
1.00E-02	192.4	188.3	180.6	187.10	5.99	155.67	4.73
5.00E-03	92.12	92.32	90.9	91.78	0.77	70.45	1.30
1.00E-03	15.77	15.63	15.51	15.64	0.13	9.93	0.25
5.00E-04	6.985	6.912	6.834	6.91	0.08	5.49	0.21
1.00E-04	1.087	1.096	1.031	1.07	0.04	0.96	0.05
5.00E-05	0.831	0.816	0.834	0.83	0.01	0.56	0.03
1.00E-05	0.331	0.331	0.336	0.33	0.00	0.25	0.00
5.00E-06	0.258	0.265	0.253	0.26	0.01	0.19	0.01
1.00E-06	0.32	0.305	0.289	0.30	0.02	0.18	0.01
5.00E-07	0.247	0.44	0.251	0.31	0.11	0.19	0.01
1.00E-07	0.242	0.249	0.258	0.25	0.01	0.20	0.01
0	0.231	0.238	0.229	0.23	0.00	0.28	0.02

Table 7: Experimental data for Figure 5.

Concentration (mg/ml)	Mean Intensity Value	Standard Deviation
20kDa Dextran		
4	214.87	29.61
3	145.84	17.60
1	67.22	3.97
0.5	57.02	3.11
0.1	48.22	1.61
150kDa Dextran		
4	135.08	18.78
3	122.33	9.57
1	75.01	11.01
0.5	74.66	6.29
0.1	56.16	3.45

Table 8: Experimental data for Figure 13.

Dextran and Direction	Tissue #1	Tissue #2	Tissue #3	Average D ($\mu\text{m}^2/\text{s}$)	Standard Deviation
20kDa – Transmural	12.55	7.41	8.51	9.49	2.71
20kDa Cross Section	23.62	15.62	21.13	20.12	4.10
150kDa Transmural	1.21	4.40	4.09	3.23	1.76
150kDa Cross Section	0.52	4.24	2.49	2.39	1.86

Table 9: Experimental data of the diffusivities calculated.

Appendix C: MATLAB CODE

C.1 Routine to Get Image Profiles

```
% Getprofiles will get transprofiles from all the images in a directory
%
% The program will display an image and wait for a response
%   If you DO NOT want to use this image, enter <x> key
%   Any other key uses this image
%
% Then it'll call the function transprofile which will get the many profiles
%   After transprofile executes, 2 figures will appear.
%   If you want to use this dataset, enter <k> key
%   If you want to SKIP to next image, enter <x> key
%
warning once

count=1;      % Index for number of Profiles
keep=[];
t=dir;

for i = 1:length(t)
    cont= '';      % Continue Variable  0 = No   1 = Yes
    % Check to make sure that the file is really an image to load
    %   if an error occurs, img is set to 1
    img = 0;
    img = eval('imread(t(i).name, ''tif'')', '1');

    if img ~= 1

        key='';

        while key ~= 'x'
            % Show figure to see if one wants to use it
            figure(100);
            imshow(img);
            colormap(hot);
            a=['Use Figure Named: ' t(i).name '?   x = no   anyotherkey = yes'];
            title(a);

            key = input('', 's');

            if key ~= 'x'

                % Get transprofile
                [profile average]=transprofile(img);

                % Input key to determine use of figure
                key = input('', 's');

                % x = exit otherwise use
                if key == 'x'
                    break
                end
            end
        end
    end
end
```

```

        end

        % k = keep data
        if key == 'k'
            keep(count).avgprofile = average;
            keep(count).numberimprof = length(profile(:,1));
            count=count + 1
        end

    end        % if
end          % while loop
end          % if
end          % for

```

C.2 Transprofile Routine

```

function [prof,avg]=transprofile(img)
% [prof, avg] = transprofile (img)
%
% transprofile() Calculates a series of image profiles
%   Asks one to select the edge boundary line then the end profile
%   Then it'll calculate a line parallel to the edge boundary and including the point
%   It'll calculate perpendicular profiels between the 2 lines
%
% @parameters image img Name of image file to get profiles
%
% @return [r,c] prof Returns a matrix of all the profiles
%   Matrix with each column being a single improfile in the rows
% @return int avg Average of all the profiles
%
% By: Jeff Hsing jhsing@mit.edu
% Last Modified Date 08/23/99

% Set Initial Variables

% Show figure to select profile
figure(1);
imshow(img);
title('Please click a transverse profile:');
colormap(hot);
hold on;

trans.intensity = 0;

while length(trans.intensity) < 5
% Get transverse profile
[trans.x trans.y trans.intensity] = improfile;
plot(trans.x, trans.y, 'w');
end

% Calculate slope and perpendicular slope
trans_st_x = trans.x(1);
trans_st_y = trans.y(1);
trans_end_x = trans.x(length(trans.x));
trans_end_y = trans.y(length(trans.y));

% Check to see if line is perpendicular
if trans_end_x == trans_st_x
    m = 'pp';
elseif trans_end_y == trans_st_y
    m = 'hz';

```

```

else
    m = (trans_end_y - trans_st_y) / (trans_end_x - trans_st_x);
    inv_m = - 1/m;           % Perpendicular Slope
end

% Get end point
title('Please click where the end of the profile should be');
[end_x end_y] = getpts;

% Caculate intercept point
interpoint = interxy(trans_st_x,trans_st_y,m,end_x,end_y);

% Plot intersect point
plot(interpoint(1),interpoint(2),'o');

% Calculate improfile of each point
np=[];
ave=[];
prof=[];

for k = 1: length(trans.x)

    newpoint=interxy(end_x,end_y,m,trans.x(k),trans.y(k));

    x=[trans.x(k) newpoint(1)];
    y=[trans.y(k) newpoint(2)];

    % Get each profile
    prof(:,k) = improfile(img,x,y);

    % Add all the profiles up
    if k == 1
        ave = prof(:,k);
    else
        ave = ave + prof(:,k);
    end

    plot(newpoint(1),newpoint(2),'w');
end

figure(2);
subplot(4,1,1);
a=strcat('Figure ');
imshow(img);
title(a);
colormap(hot);

subplot(4,1,2);
plot(trans.intensity);
title('Transverse profile');

avg=ave/length(trans.x);

subplot(4,1,3);
plot(avg);
title('Average');

subplot(4,1,4);
plot(s_peak(avg));
title('Shifted Average');

```

```

%=====

function ans = interxy(x1,y1,m,x2,y2)
% interxy(x1,y1,m,x2,y2) gets the intersection point given a
% a line described by x1,y1 and slope m
% and a point x2,y2

if m == 'pp'           % Check to see if it's perpendicular
    ans = [x1 y2];
elseif m == 'hz'      % Check to see if it's horizontal
    ans = [x2 y1];
else
    % Set up into matrix [a b ; c d] * [x ; y] = [e ; f]
    a=[m -1 ; 1/m 1];
    b=[(m*x1 - y1) ; (y2 + x2/m)];

    % Solve matrix to find intersection
    ans=a\b;           % Intersecting Point
end

```

C.3 Shifts Profile Routine to Remove Initial Uprise

```

function sp=shiftprofile2(p, threshold, debugging)
% Shiftprofile2(p, threshold, debugging)
%
% Shiftprofile2() will shift the profile by removing the initial rising points
% The algorithm uses the derivative of the average profile and
% then looks for the maximum derivative and then selects the first point
% that is below the slope threshold. The initial profile is shifted over
% that many points.
%
% @parameter profile p Profile to shift
% Data structure of profile
% profile.avgprofile = average improfile
% profile.numberimprof = number of improfiles in average
% @parameter int threshold Threshold for slope (default = 0)
% @parameter int debugging Set to 1 if you want graphs to be plotted (default = 0)
%
% @return profile Returns shifted profile
%
% Written by : Jeff Hsing jhsing@mit.edu
% Last Modified: May 9, 2000
%

if nargin < 3
    debugging = 0;
end

if nargin < 2
    threshold = 0;
end

if debugging == 1
    figure;
end

for i = 1 : length(p)

    % Find the first derivative and the find the first point
    % after the max that meets threshold
    temp = diff(p(i).avgprofile);
    [maxvalue,maxindex] = max(temp);

```

```

for j = maxindex : length(temp);
    if temp(j) < threshold
        index = j;
        break;
    end
end

len=length(p(i).avgprofile);

% Shift profile over
sp(i).avgprofile(1:len-index+1) = p(i).avgprofile(index:len);
sp(i).numberimprof=p(i).numberimprof;

% show progress only if debugging = 1
if debugging == 1
    subplot(3,1,1);
    plot(p(i).avgprofile);
    axis ([0 50 0 250]);
    title(['Profile # ' num2str(i)]);

    subplot(3,1,2);
    plot(diff(p(i).avgprofile));
    axis ([0 50 0 50]);

    subplot(3,1,3);
    plot(sp(i).avgprofile);
    axis ([0 50 0 250]);
    title(['Removed ' num2str(index) ' points']);

    pause;
end
end

```

C.4 Converts Intensity to Tissue Concentration

```

function [tConc] = jh_int2tconc(tissint,m,b,mw,e);
% tConc = jh_int2tconc(tissint, m, b, mw, e)
%
% jh_int2tconc() Converts tissue intensity profile to tissue concentration
%
% @parameter int[] tissint Tissue intensity profile
% @parameter int m Slope of intensity to bulk fluid relationship
% @parameter int b Y-intercept of intensity to bulk fluid relationship
% @parameter int mw Molecular weight of compound used
% @parameter int e Fractional Free Space of compound in tissue
%
% @return int[] tConc Tissue Concentration in [# compound / ml tissue]
%
% Written by : Jeff Hsing jhsing@mit.edu
% Last Modified: May 9, 2000
%
% converts intensity to bulk fluid concentration
bConc = (tissint - b) / m;

% converts bulk fluid concentration to number of compound
mConc = bConc * (1/mw) * (1/1000) * (6.022E23);

% converts bulk fluid concentration to tissue concentration
tConc = mConc * e;

```

C.5 Diffusion Model in 1-D

```

function [simC, simX] =
diff1d(D,tissuelength,nunits,eps,cleft,cright,totalltime,ninc,conv)
% Diff1d will calculate and return the concentration profile
% Inputs (D, tissuelength, nunits, eps, cleft, cright, totalltime,
%         ninc, conv)
%
%
% Written by: Jeff Hsing
% Last Modified 2/28/00
%
% (c) Copyright 1999 by Jeff Hsing
%
% D                diffusivity (um^2/s)
% tissuelength     length of tissue in um
% nunits           number of units in tissuelength
% eps              Epsilon Fractional Free Space
% cleft            concentration at left (mg/ml)
% cright           concentration at right (mg/ml)
% totalltime       total length of time to calculate (min)
% ninc             number of time increments
% conv             convection
%
% Calculate other variables needed from input

dx = tissuelength/nunits;           % Step size (um)
x = [dx:dx:tissuelength-dx]';      % x-grid points, (interior)
n = length(x);                      % Size of Matrix
dt = (totalltime*60)/ninc;          % Time step (in sec)
g = D*dt/dx^2;                      % unknown term for now.
b = conv*dt/dx;                    % Terms for convection

% Construct matrices A(+g) and A(-g)
Ap= sparse(diag((1+g+(b/2))*ones(n,1)) - ...
           diag(ones(n-1,1),1)*g/2 - ...
           diag(ones(n-1,1),-1)*((g/2)+(b/2)) );

Am = sparse(diag((1-g-(b/2))*ones(n,1)) + ...
           diag(ones(n-1,1),1)*g/2 + ...
           diag(ones(n-1,1),-1)*((g/2)+(b/2)));

C = zeros(n,ninc);                 % Start with all zeros for C

% The right-hand-side vector b
b=g*[cleft zeros(1,n-2) cright]';

% Calculate each subsequent time
for t=1:ninc                        % For totalltime length
    C(:,t+1) = Ap\(Am*C(:,t)+b);
end

simC = [cleft; C(:,ninc+1)];
length(simC);
simX = 0:dx:tissuelength-dx;
length(simX);
return

```

C.6 Fit Simulated Concentration Profile to Experimental Profile

```
function [paramfit,rmserror] = fitprofile(profile,totaltime,cleft,paramorig,dt,nodes);

global imConcNA
if (nargin < 6)
    dt = 10;
    nodes = 40;
end;

% Function fitprofile.m
%
% Use: [paramfit,rmserror] = fitprofile (path,file,paramorig,fitwhich,dt,nodes,algo);
%
% * paramorig = [Cev Cpv Rend Radv Eps D V totalmin]; ==> INITIAL PARAMETERS with
units:
%   Cev, Cpv:   endo and perivascular baths, mg/mL
%   Rend, Radv: intimal and adventitial resistances, sec/um
%   Eps:        fractional free space, dimensionless
%   D:          diffusivity, um^2/sec
%   V:          convective velocity, um/sec
%   totaltime: total simulation time, min
% * dt = step time in seconds
% * nodes = number of nodes used to represent media in computed profile
% * algo = 'cn' ==> use Crank-Nicholson.
%
% Given initial parameters and the path and filename containing an experimental data
% tissue concentration profile, returns
% (1) paramfit = the values of the parameters in fitwhich representing the best fit
%     through the data.
% (2) rmserror = ... mean square error of the fit given the paramfit values
% Originally written by Chao-Wei Hwang
% Modified by Jeff Hsing  jhsing@mit.edu

algo = 'cn';
fitwhich = ('D');

if (nargin < 2)
    totaltime = 240;    % default time is 4 hours
end

if (nargin < 4)
    cright = min(profile);
    if cright < 0
        cright = 0;
    end
    paramorig = [cleft 0 0 0 0.33 6 0 totaltime];
end

% Scale is the image scale converting pixels to length
% Units of pixles/mm
scale=151;

% Extract the inital values of the parameters
Cev = paramorig(1)
Cpv = paramorig(2)
Rend = paramorig(3);
Radv = paramorig(4);
Eps = paramorig(5);
D = paramorig(6);
V = paramorig(7);
totalmin = paramorig(8);
```

```

strfitwhich = '';

% Extract the parameters indicated by fitwhich to be varied in the fit
paramvary(i) = D;

% Extract out the experimental tissue concentration profile
tissconc = profile;

% -----
% Fit the data. Find the best fit for paramvary parameters, and store in paramfit.
% -----

defaultopt=foptions;
paramfit=fmins('cnerror',paramvary,defaultopt,[],paramorig,fitwhich,tissconc,dt,nodes)
;
disp(['Minimization routine completed. Displaying final fit...']);
rmsererror=cnerror(paramfit,paramorig,fitwhich,tissconc,dt,nodes);

% -----
% DISPLAY RESULTS
% -----

% Extract values of fitted variables from paramfit
D = paramfit(1);

% Compute theoretical curve again
Lmed = length(tissconc)*1.326; % um (length of media)
dx = Lmed/nodes; % um
verbose = 0;

[simC, simX] = diffld (D,length(tissconc) / scale * 10^3, nodes, Eps, Cev, Cpv,
totalmin, 1200,0);

dx = 1/ scale * 10^3;
tissX = 0 : dx : (length(tissconc)-1) * dx;
tissconc_interp = (interp1(tissX,tissconc,simX))';

%hold on;
figure;
plot(simX,simC,'m',simX,tissconc_interp,'b');
legend('Best Fit','Data');
xlabel('Distance from the Intima (um)');
ylabel('Tissue Concentration (#/mL)');
title([' Best fit: [' strfitwhich ' ] = [' num2str(paramfit) ' ]]);
hold off;

disp(['Original values: [Cev Cpv Rend Radv Eps D V totalmin]']);
disp(['= [' num2str(paramorig) ' ]']);
disp(['Fitted values: [' strfitwhich ' ] = [' num2str(paramfit) ' ]']);
disp(['Root mean squared error = ' num2str(rmserror)]);

```

C.7 Error Function Between Experimental Data and Simulated Data

```

function rmserror=cnerror(paramvary,paramorig,fitwhich,tissconc,dt,nodes)
% Function cnerror.m
%
% Use: rmserror = cnerror(paramvary,paramorig,fitwhich,tissconc,dt,nodes);
%
% Originally written by Chao-Wei Hwang

```



```

% Modified by Jeff Hsing

% Extract the initial values of the parameters
Cev = paramorig(1);
Cpv = paramorig(2);
Rend = paramorig(3);
Radv = paramorig(4);
Eps = paramorig(5);
D = paramorig(6);
V = paramorig(7);
totalmin = paramorig(8);

scale = 151;      % Number of pixels per mm

% Extract variables to be varied from paramvary as indicated by fitwhich, and
% re-assign those new values to the appropriate variables.
D = paramvary(i);

if min(paramvary)<0
    rmerror = 10000;
    disp(['NEGATIVE PARAMETERS: [' D ']=[' num2str(paramvary) ']]);
else

    % With the given parameters, compute profile simC.  Vector simX denotes the
    % position from intima of each point in simC.  Each point in the computed
    % profile is dx microns apart, starting at 0 microns from intima.

    % tissue length
    a = length(tissconc) / scale * 10^3;

    [simC,simX] = diff1d(D,a,nodes,Eps,Cev,Cpv,totalmin,1200,0);

    % Now, find the points in the data profile corresponding to the micron position
    % of the computed points.  If the computed point falls between 2 data points, a
    % new data point is found at the micron position of the computed point by a
    % linear interpolation of the two closest data points.
    % dataX = [0:length(tissconc)-1]*1.326;
    %error here... way too many points

    % Now we need to find the the position versus concentration of data points inputed
as tissconc
    % tissX = distance away from source in um
    dx = 1/ scale * 10^3;
    tissX = 0 : dx : (length(tissconc)-1) * dx;

    % Now we interpolate the tissue data onto the model data
    tissconc_interp = (interp1(tissX,tissconc,simX))';
    t_last = tissconc_interp (length(tissconc_interp));
    if ( (t_last>0) | (t_last<0) | (t_last==0) )

    else
        tissconc_interp(length(tissconc_interp)) =
tissconc_interp(length(tissconc_interp) - 1);
    end

    % Compute root mean squared error
    rmerror = sqrt(mean((simC-tissconc_interp).^2));
    disp(['[' strfitwhich ']= [' num2str(paramvary) ']=> rmserr: '
num2str(rmerror)]);

end % if

```

References

- American Heart Association. "Achievements in Public Health, 1900-1999: Decline in Deaths from Heart Disease and Stroke – United States, 1900-1999". CDC MMWR Weekly. **48** (30); 649-656.
- Arras M, Mollnau et al. "The delivery of angiogenic factors to the heart by microsphere therapy". Nature Biotechnology. **15**:Feb: 159-162.
- Avitall B, Hare J, Zander G et al. "Iontophoretic Transmyocardial Drug Delivery: A Novel Approach to Antiarrhythmic Drug Delivery". Circulation, **85**:4. 1582-1593.
- Bailey SR. "Local Drug Delivery: Current Application". Progress in Cardiovascular Diseases, **40** (2), 183-204.
- Crank J. The Mathematics of Diffusion. Oxford University Press, New York. 1975
- Crick SJ, Sheppard MN et al. "Anatomy of the pig heart: comparisons with normal human cardiac structure". J Anat. **193**: 105-119.
- Edelman ER, Lovich M. "Drug Delivery Models Transported to a New Level". Nature Biotechnology. **16**: 136-137. (1998)
- Edelman ER, Nugent MA, Karnovsky MJ. "Perivascular and intravenous administration of basic fibroblast growth factor: Vascular and solid organ deposition". Proc. Natl. Acad. Sci, **90**: 1513-1517.
- Elmalak O, Lovich MA, Edelman ER. "Correlation of Transarterial Transport of Various Dextran with their Physicochemical Properties". Biomaterials in Press 2000.
- Feldman HS, Hartvig P et al. "Regional Distribution of ¹¹C-Labeled Lidocaine, Bupivacaine, and Ropivacaine in the Heart, Lungs, and Skeletal Muscle of Pigs Studied with Positron Emission Tomography". Biopharm and Drug Disp, **18**:2, 151-164 (1997).
- Fluck DS, Etherington PJ, Sheridan DJ, Winlove CP. "Solute Exchange in the Rabbit Myocardium: Ischaemia, Reflow, and Myocardial Necrosis". Basic Res Cardiol, **93**: 354-360 (1998).
- Haunso S, Sejrsen P, Svendsen JH. "Transport of Beta-blockers and Calcium Antagonists by Diffusion in Cat Myocardium". J Cardiovasc Pharm, **17**: 357-364, (1991).

- Host NB, Sejrsen P, Jensen LT, Haunso S. "Diffusional transport of the Aminoterminal Propeptide of the Type III procollagen in the Interstitium of the Globally Ischaemic Cat Myocardium". Clinica chimica Acta, **255**: 183-194, (1996).
- Katz, AM. Physiology of the Heart. 2nd ed. Raven Press, NY 1992.
- Kornowski R, Fuchs S, et al. "Delivery Strategies to Achieve Therapeutic Myocardial Angiogenesis". Circulation. **101**:454-458. (2000)
- Kreyszig, Erwin. Advanced Engineering Mathematics. 7th ed. John Wiley & Sons, New York. 1993.
- Langman, Jan. Medical Embryology. 4th ed. Williams & Wilkins. Baltimore. 1981.
- Lopez JJ, Edelman ER, et al. "Basic Fibroblast Growth Factor in a Preclinical Model of Chronic Myocardial Ischemia: A Comparison of Angiographic Echocardiographic and Coronary Flow Parameters". J Pharm Exp Ther. **282**: 385-390.
- Lovich MA, Edelman ER. "Mechanisms of Transmural Heparin Transport in the Rat Abdominal Aorta After Local Vascular Delivery". Circulation Research. **77**: 1143-1150 (1995).
- Lovich MA, Edelman ER. "Computational Simulations of Local Vascular Heparin Deposition and Distribution". Am. J. Physiol. **271**: H2014-H2024 (1996).
- Moore, Keith. The Developing Human: Clinically Oriented Embryology. 4th ed. WB Saunders Co. Philadelphia. 1988.
- National Heart, Lung and Blood Institute. "Morbidity & Mortality: 1998 chartbook on cardiovascular, lung, and blood diseases". Rockville, MD: US Department of Health and Human Services, National Institutes of Health, 1998.
- Nemoto and LaManna. Oxygen Transport to Tissue XVIII, Plenum Press, New York, 1997.
- Popel AS. "Theory of Oxygen Transport to Tissue". Crit Rev in Biomed Engr. **17**: 3: 257-321.
- Tice T, Staas J. "Getting to the Heart of Growth Factor Delivery". Nature Biotechnology, **16**: 134. (1998).
- Van Beek JH, Loisel DS, Westerhof N. "Calculation of oxygen diffusion across the surface of isolated perfused hearts". Am. J. Physiol. **263**: H1003-H1010.
- Wade WK. "Quantification of the Distribution of Macromolecules in Vascular Tissue". Master's Thesis. MIT February 1998.
- Wade WK, Lovich MA et al. "Measurement of Drug Distribution in Vascular Tissue Using Quantitative Fluorescence Microscopy". J. Pharm Science. **88**(8): 822-829.

Weaver ME, Pantely GA et al. "A quantitative study of the anatomy and distribution of coronary arteries in swine in comparison with other animals and man", Cardiovasc Res. **20**: 907-917.

Wolpers HG, Hoefl A et al. "Transport of inert gases in mammalian myocardium: comparison with a convection-diffusion model". Am. J. Physiol. **259**: H167-H173.